M2-like macrophages are responsible for collagen degradation through a mannose receptor–mediated pathway

Daniel H. Madsen,[1,4] Daniel Leonard,[1] Andrius Masedunskas,[2] Amanda Moyer,[1] Henrik Jessen Jürgensen,[1,4] Diane E. Peters,[1,7] Panomwat Amornphimoltham,[2] Arul Selvaraj,[1] Susan S. Yamada,[3] David A. Brenner,[5] Sven Burgdorf,[6] Lars H. Engelholm,[4] Niels Behrendt,[4] Kenn Holmbeck,[3] Roberto Weigert,[2] and Thomas H. Bugge[1]

[1]Proteases and Tissue Remodeling Section and [2]Intracellular Membrane Trafficking Unit, Oral and Pharyngeal Cancer Branch, and [3]Matrix Metalloproteinase Section, National Institute of Dental and Craniofacial Research, National Institutes of Health, Bethesda, MD 20892
[4]The Finsen Laboratory, Rigshospitalet/Biotech Research and Innovation Centre, University of Copenhagen, 2100 Copenhagen, Denmark
[5]Department of Medicine, University of California, San Diego, La Jolla, CA 92093
[6]Life and Medical Sciences Institute, University of Bonn, 53115 Bonn, Germany
[7]Program of Pharmacology and Experimental Therapeutics, Sackler School of Graduate Biomedical Sciences, Tufts University School of Medicine, Boston, MA 02111

Tissue remodeling processes critically depend on the timely removal and remodeling of preexisting collagen scaffolds. Nevertheless, many aspects related to the turnover of this abundant extracellular matrix component in vivo are still incompletely understood. We therefore took advantage of recent advances in optical imaging to develop an assay to visualize collagen turnover in situ and identify cell types and molecules involved in this process. Collagen introduced into the dermis of mice underwent cellular endocytosis in a partially matrix metalloproteinase–dependent manner and was subsequently routed to lysosomes for complete degradation. Collagen uptake was predominantly executed by a quantitatively minor population of M2-like macrophages, whereas more abundant *Col1a1*-expressing fibroblasts and *Cx3cr1*-expressing macrophages internalized collagen at lower levels. Genetic ablation of the collagen receptors mannose receptor (*Mrc1*) and urokinase plasminogen activator receptor–associated protein (Endo180 and *Mrc2*) impaired this intracellular collagen degradation pathway. This study demonstrates the importance of receptor-mediated cellular uptake to collagen turnover in vivo and identifies a key role of M2-like macrophages in this process.

Introduction

Morphogenesis, tissue remodeling, and tissue repair all require the targeted remodeling of interstitial and basement membrane collagen to allow for organ growth, cell migration, and translation of contextual cues that are embedded within the extracellular matrix. Perturbed collagen homeostasis underlies a remarkable array of important human diseases, including fibrosis, that are attributable to excess interstitial deposition of collagen and degenerative diseases, such as osteoporosis, osteoarthritis, and rheumatoid arthritis, which are characterized by a loss of collagen from tissues. Finally, the ability of tumor cells to leave their site of origin and seed at novel locations is dependent on their ability to orchestrate the local degradation of collagen (Joyce and Pollard, 2009; Rowe and Weiss, 2009; Kessenbrock et al., 2010). Understanding the precise mechanisms underlying normal and abnormal collagen homeostasis is, therefore, of significant basic biological and clinical importance.

The mechanisms of collagen turnover have been the subject of extensive studies over the past several decades, and two mechanistically different collagen catabolic pathways have been proposed: an extracellular pathway, in which collagen is degraded by membrane-bound and soluble proteases, and an endocytic pathway, in which collagen is first internalized by cells and then

D.H. Madsen and D. Leonard contributed equally to this paper.

Correspondence to Thomas H. Bugge: thomas.bugge@nih.gov

Abbreviations used in this paper: GM-CSF, granulocyte M-CSF; M-CSF, macrophage colony-stimulating factor; MMP, matrix metalloproteinase; MR, mannose receptor; PA, protective antigen; uPARAP, urokinase plasminogen activator receptor–associated protein.

The Rockefeller University Press $30.00
J. Cell Biol. Vol. 202 No. 6 951–966
www.jcb.org/cgi/doi/10.1083/jcb.201301081

degraded by lysosomal cysteine proteases (Aimes and Quigley, 1995; Everts et al., 1996; Lauer-Fields et al., 2002; Hotary et al., 2006; Lee et al., 2006; Madsen et al., 2007; Krane and Inada, 2008; Lecaille et al., 2008; Messaritou et al., 2009; Segovia-Silvestre et al., 2009; Bugge and Behrendt, 2011). The existence of the latter pathway for collagen turnover in vivo is primarily supported by electron microscopy studies showing an abundance of collagen fibers in the endosomal and lysosomal compartments of mesenchymal cells presumed to be engaged in connective tissue degradation during cancer invasion, articular cartilage destruction in rheumatoid arthritis, bone resorption in periodontal disease, periodontal ligament turnover, and uterine involution (Cullen, 1972; Beertsen and Everts, 1977; Harris et al., 1977; Soames and Davies, 1977; Jurukova and Milenkov, 1981; Neurath, 1993; Lucattelli et al., 2003; Ryvnyak and Dulgieru, 2003). However, other studies have suggested that the observed intracellular collagen does not reflect the actual degradation of collagen derived from the extracellular matrix but rather consists of misfolded collagen that has been rerouted for immediate lysosomal degradation during the synthesis process (Bienkowski et al., 1978; Berg et al., 1980). Furthermore, considerable gaps in knowledge also exist as to the specific mechanisms by which collagen would be endocytosed and routed for lysosomal degradation. This particularly regards the requirement for collagenase cleavage before cellular uptake, the identity of cells endowed with the capacity to internalize and degrade collagen intracellularly, and the cellular receptors that mediate the initial collagen uptake. With respect to the latter, the collagen binding $\alpha1\beta1$ and $\alpha2\beta1$ integrins were the first proposed collagen internalization receptors, based on the observation that integrin-blocking antibodies impair the uptake of collagen-coated beads by cultured fibroblasts (Arora et al., 2000; Segal et al., 2001). A role of milk fat globule epidermal growth factor 8 in opsonizing collagen for specific uptake by macrophages was also recently proposed (Atabai et al., 2009). Furthermore, two members of the mannose receptor (MR) family of endocytic recycling receptors, the MR (*MRC1* and CD206) and the urokinase plasminogen activator receptor–associated protein (uPARAP; endo180, *MRC2*, and CD280), were shown to aggressively internalize and target an assortment of collagen types for lysosomal degradation by cultured cells (Engelholm et al., 2003; Wienke et al., 2003; Martinez-Pomares et al., 2006; Madsen et al., 2011).

Cognizant of these considerable mechanistic gaps in the knowledge of collagen turnover in vivo, we took advantage of recent advances in optical microscopy to develop a novel assay to directly visualize the fate of exogenous collagen introduced to the mouse dermis. By using this assay, we were able to characterize the cell types and molecules engaged in collagen degradation in vivo. Most importantly, we identify MR-dependent intracellular collagen degradation by M2-like macrophages as a novel and dominant collagen turnover pathway.

Results

Generation of an assay to visualize intracellular collagen degradation in vivo

Acid-extracted rat tail tendon type I collagen fibrils self-assemble within minutes to form native, trypsin-resistant collagen fiber networks when incubated at physiological pH in vitro. Collagen networks formed this way have been used extensively as a model system to study cellular collagen turnover by cells explanted ex vivo (Birkedal-Hansen et al., 2003). To determine whether similar collagen networks could be reconstituted in vivo and then be visualized in situ, we fluorescently labeled acid-extracted rat tail tendon type collagen I with either Alexa Fluor 488, 594, or 647, which are highly photostable and pH-insensitive fluorescent dyes (see Materials and methods for details on this and other procedures; Panchuk-Voloshina et al., 1999). These fluorescently labeled collagen fibrils preserved their ability to rapidly form trypsin-resistant, collagenase-sensitive collagen networks ex vivo (Fig. 1 A and not depicted). Importantly, when neutralized from an acidic solution and then immediately injected into the subcutaneous space of mice, the fluorescently labeled collagen fibrils self-assembled to form similar collagen networks within the mouse dermis. These networks either formed around preexisting endogenous collagen/elastin bundles, or they formed de novo, independent of existing matrix scaffolds. In both cases, they easily could be visualized by either two-photon microscopy (not depicted) or confocal fluorescence microscopy of the exposed ventral dermis (Fig. 1, B–D). Fortuitously, the collagen injection procedure disrupted dermal homeostasis, as revealed by a substantial influx of cells into the injection field (Fig. 1 E) and by a large increase in the expression of genes associated with matrix turnover 24 h after injection, including genes encoding collagenases and gelatinases (Fig. 1 F). Furthermore, the introduced collagen appeared to be continuously degraded with an approximate half-life of 3.4 d, as determined by extraction of fluorescent material from injected skin (Fig. 1 G). Collectively, this suggested that the tissue damage inflicted by the subcutaneous collagen placement procedure creates a matrix catabolic microenvironment, thereby potentially making it possible to study the degradation of the exogenously introduced collagen networks in situ. By coinjecting the collagen with 10-kD dextran fluorescently labeled with Texas red, the lysosomal compartment of cells could be visualized (Fig. 1 H; Sandoval et al., 2004; Masedunskas and Weigert, 2008). Likewise, intravenous injection of the mice with fluorescent Hoechst 33342 dye 4–6 h before imaging allowed for easy visualization of cell nuclei (Fig. 1 H). A representative example of the appearance of an injection field reconstituted from serial z stacks is shown in Video 1.

Exogenously introduced collagen undergoes cellular internalization and is routed to lysosomes

Inspection of the collagen-injected area by confocal fluorescence microscopy revealed numerous cells displaying perinuclear endocytic vesicles containing fluorescently labeled collagen, indicative of vigorous cellular uptake of exogenous collagen in vivo (Fig. 2 A). Indeed, a systematic quantitative analysis of the injection areas reconstituted from serial z stacks showed that >90% of the dextran-uptaking cells also contained internalized collagen (see following paragraph). Importantly, these collagen-containing endocytic vesicles included

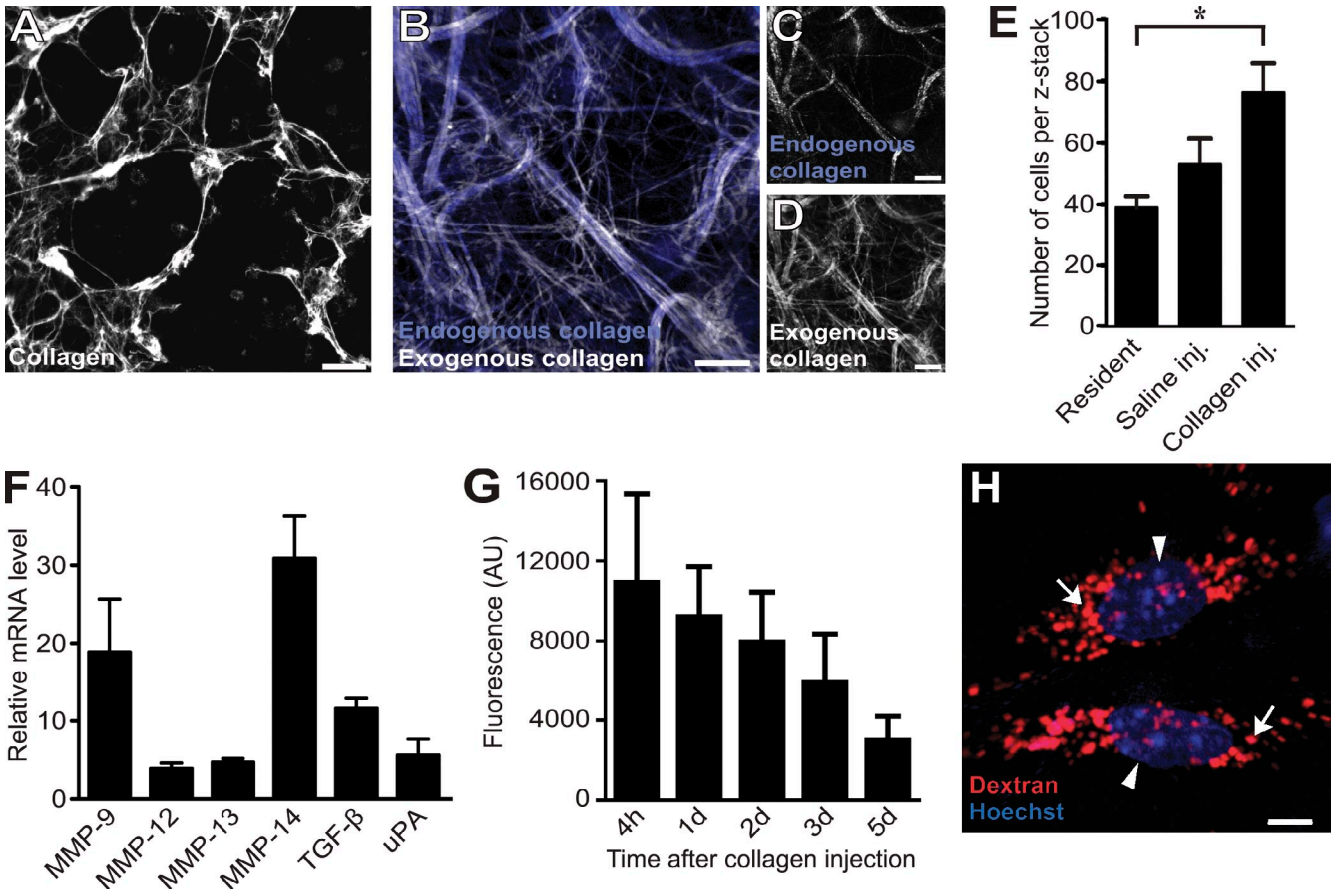

Figure 1. **An assay to visualize intracellular collagen degradation in situ.** (A–D) Microscopic appearance of collagen fibers formed after incubation of Alexa Fluor 647–labeled acid-extracted rat tail tendon type I collagen at neutral pH in vitro (A) or formed in vivo 24 h after injection into the dermis of live mice (B–D). Dermal-injected fluorescently labeled rat tail collagen fibrils form collagen fiber networks (white fibers in B) that may be associated with existing collagen/elastin scaffolds (blue fibers in B and white fibers in C, visualized by confocal microscopy) or may form ab initio (compare C and D). (E–G) Dermal collagen injection disrupts tissue homeostasis and generates a matrix catabolic environment. (E) Total cell counts in noninjected (left bar), vehicle-injected (middle bar), or collagen-injected (inj.; right bar) dermis, as determined by the counting of nuclei in four to six serial z stacks from the injection field. $n = 3$ for each treatment. *, $P < 0.05$, Student's t test, two tailed. (F) Quantitative PCR analysis of mRNA levels of six genes associated with extracellular matrix remodeling in the dermis of collagen-injected mice. Data are expressed as fold increase relative to noninjected mice. $n = 3$ for noninjected and for collagen-injected mice. uPA, urokinase-type plasminogen activator. (G) Total fluorescence extracted at the indicated time points from skin of mice injected with Alexa Fluor 488–conjugated collagen. $n = 4$ for each time point. AU, arbitrary unit. (H) Visualization of the lysosomal compartment (red; examples with arrows) and nuclei (blue; arrowheads) of cells in dermal injection fields by local injection with Texas red 10-kD dextran and systemic injection of Hoechst dye, respectively, 24 and 4–6 h before imaging. Data are shown as means ± SD. Bars: (A–D) 10 µm; (H) 5 µm.

lysosomes, as shown by the frequent colocalization of collagen and dextran (Fig. 2, B–D), demonstrating that internalized collagen is routed to the lysosomes. Imaging of dermis distant from the injection site revealed that the injected collagen remained localized to the area of injection, whereas trace amounts of dextran occasionally were detected (Fig. 2 E). Fluorescently labeled collagen injected in the absence of dextran displayed a similar vesicular distribution as observed when coinjected with the dextran, demonstrating that the dextran is not affecting the uptake of collagen (Fig. 2 F). The routing of internalized collagen to the lysosomes is consistent with previous data showing that fluorescently labeled collagen internalized by cultured cells is directed to the lysosomes (Kjøller et al., 2004). In previous studies, we have shown that inhibition of lysosomal cysteine proteases leads to increased levels of internalized collagen in both macrophages and fibroblasts, providing evidence that the internalized collagen is lysosomally degraded (Kjøller et al., 2004; Madsen et al., 2011). To directly examine the fate of internalized collagen, we allowed cultured fibroblast to internalize radiolabeled collagen and subsequently analyzed the physical state and the location of the collagen as a function of time by TCA precipitation of cell lysates and culture supernatants (Fig. 2 G). 5 h after collagen exposure, 59% of the radioactivity was in a cell-associated and already non-TCA–precipitable form, showing vigorous degradation of internalized collagen. After 9 h, most of this degraded collagen was released from cells and accumulating in the medium, with only 9% remaining cell associated in a TCA-precipitable form. A similar or even more efficient lysosomal collagen degradation process by professional phagocytes such as macrophages would be expected.

We next determined the effect of inhibiting metalloproteinase activity, including pericellular/extracellular matrix metalloproteinase (MMP) activity, on cellular collagen uptake, by treating mice with the broad-specificity metalloproteinase inhibitor GM6001 (Grobelny et al., 1992) before collagen,

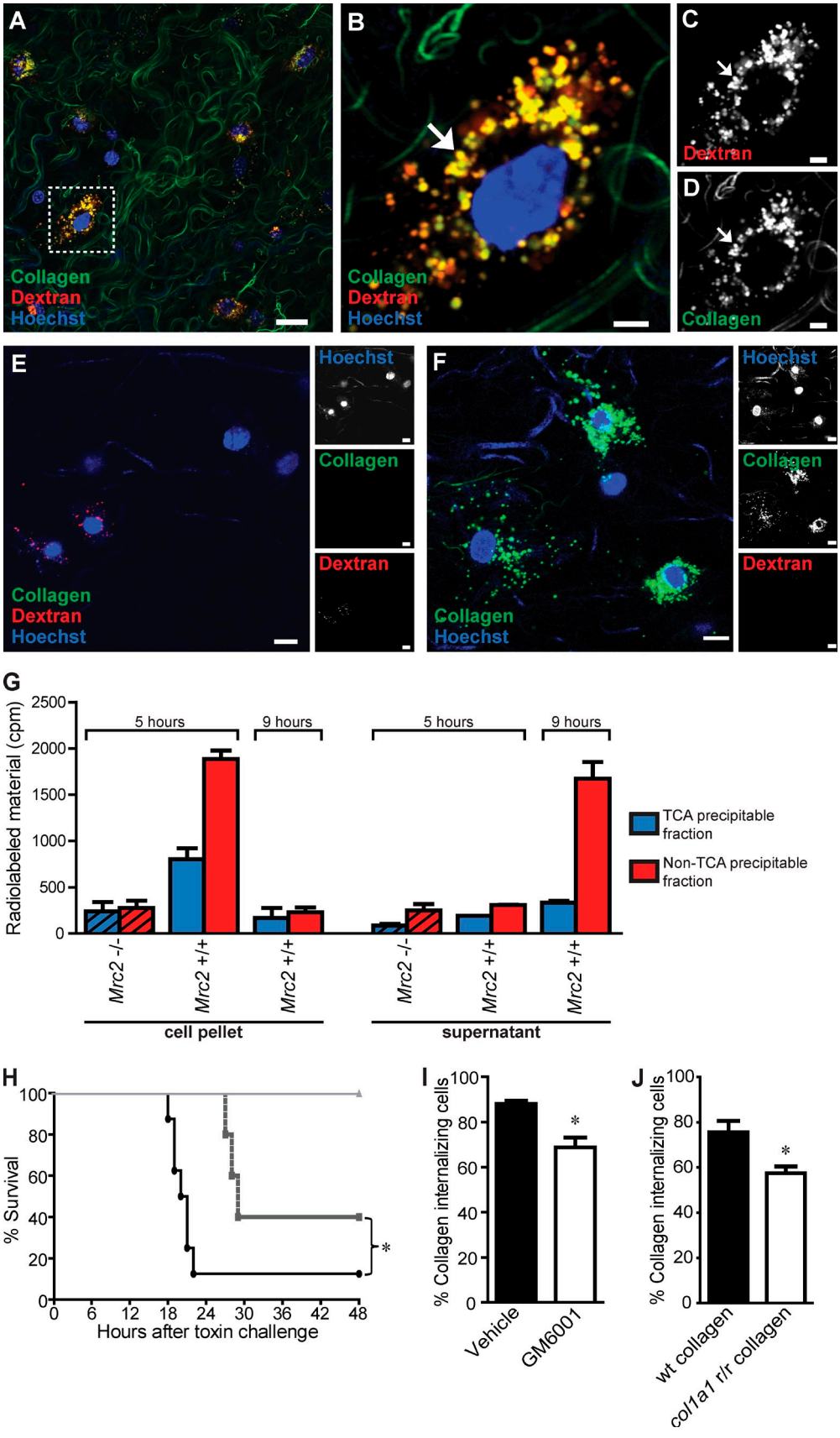

Figure 2. **Cellular uptake and lysosomal routing of collagen in vivo.** (A) Representative image of mouse dermis 24 h after injection shows vigorous cellular uptake of collagen, as revealed by multiple cells presenting with fluorescently labeled collagen located within perinuclear endocytic vesicles. (B–D) High magnification of a single collagen-uptaking cell (box in A), illustrating the frequent colocalization of collagen and Texas red dextran

dextran, and Hoechst dye injections. As expected, this treatment regimen inhibited metalloproteinase activity, as shown by the partial protection afforded to mice challenged with a lethal dose of an MMP-activated modified anthrax toxin (Fig. 2 H; Liu et al., 2000). The GM6001 treatment resulted in a small, but significant, reduction in the fraction of cells internalizing collagen from 88% of dextran-uptaking cells in the injection field to 69% (Fig. 2 H). As an independent approach, we also injected mice with tail tendon collagen isolated from mice with a targeted mutation in the *Col1a1* gene (*Col1a1*$^{r/r}$ mice), which results in the generation of collagenase-resistant collagen type I (Liu et al., 1995). The cellular uptake of this mutant collagen was compared with collagen isolated from littermate wild-type mice. A significant reduction (from 75 to 57%) in the fraction of cells internalizing *Col1a1*$^{r/r}$ collagen compared with wild-type collagen was observed (Fig. 2 J). Collectively, this suggests that MMP cleavage facilitates the cellular uptake of collagen.

Low-level collagen uptake by Cx3cr1-GFP–positive macrophages and Col1a1-GFP–positive fibroblasts

Having established that intracellular collagen degradation is a functional collagen turnover pathway in vivo, we next set out to identify the specific cell types that engage in the intracellular degradation pathway in vivo. For this purpose, we took advantage of the previous generation of two transgenic mouse strains with macrophages or fibroblasts expressing fluorescent proteins amenable to imaging in vivo. We first injected transgenic mice carrying one wild-type and one GFP-tagged *Cx3cr1* allele with fluorescent collagen, dextran, and Hoechst dye as described in the previous section. These mice express GFP in most tissue macrophages but are phenotypically normal and therefore well suited for this experiment (Jung et al., 2000; Arnold et al., 2007). Analysis of dermal injection fields showed numerous rounded GFP-positive cells containing internalized collagen located within the lysosomal compartment. Enumeration of cellular collagen uptake 24 h after dermal collagen injection by analysis of serial z stacks from the injection fields showed that on average 49% of cells displaying collagen in endocytic vesicles were GFP positive, whereas 51% were GFP negative (Fig. 3, A and C). Intracellular collagen was observed in 79% of all GFP-positive cells located in the dermis, whereas 21% of the GFP-positive cells were collagen negative (Fig. 3 D). No obvious morphological difference was observed between collagen internalizing and noninternalizing GFP-positive cells (unpublished data).

We next used a similar strategy to determine the contribution of fibroblasts to collagen internalization. Mice carrying a *Col1a1*-GFP transgene express the recombinant fluorescent protein in dermal fibroblasts and in type 1 collagen-producing cell populations at various other sites (Krempen et al., 1999). These mice were injected with the aforementioned fluorescent collagen, dextran, and Hoechst dye. Analysis of serial z stacks from the injection fields of these mice showed that on average 37% of cells displaying collagen in endocytic vesicles were GFP positive, whereas 63% of cells displayed intracellular collagen and were GFP negative (Fig. 3, B and F). Overall, 95% of GFP-positive cells in the injection fields of *Col1a1*-GFP transgenic mice displayed intracellular collagen, whereas 5% did not (Fig. 3 G). Collectively, these data directly demonstrate that both macrophages and fibroblasts engage in intracellular collagen degradation in vivo.

To address whether these two cell types were resident in the dermis or were being recruited upon the introduction of collagen, we determined the number of GFP-positive and GFP-negative cells in the dermis of *Cx3cr1*-GFP transgenic mice (Fig. 3 E) and in *Col1a1*-GFP transgenic mice (Fig. 3 H) in the presence and absence of exogenous collagen. This analysis showed that essentially all *Cx3cr1*-GFP–positive cells were recruited, whereas the *Col1a1*-GFP–positive cells resided in the dermis before exogenous collagen placement.

M2-like macrophages vigorously internalize collagen

Analysis of injection fields from either *Cx3cr1*-GFP or *Col1a1*-GFP transgenic mice revealed a distinct population of GFP-negative cells that displayed very high levels of internalized collagen, when compared with all GFP-positive cells (unpublished data). To further investigate this confounding observation, we interbred *Cx3cr1*-GFP and *Col1a1*-GFP transgenic mice and characterized the collagen-internalizing GFP-positive and -negative cells in the ensuing double-transgenic offspring (Fig. 4). Interestingly, a residual population of GFP-negative cells (15% of all cells) still displayed intracellular collagen (Fig. 4, A and B). Furthermore, these collagen-internalizing, GFP-negative cells were immediately distinguishable from all GFP-labeled cells in inspected injection fields by the size and number of their lysosomes and by their accumulation of much larger quantities of collagen in endocytic vesicles (Fig. 4 A and see Fig. 7 A), suggesting that this subfraction of GFP-negative cells prominently contributes to collagen turnover in the dermis. Indeed, quantitative

in perinuclear vesicles (yellow; examples with arrows), indicative of lysosomal routing of endocytosed collagen. (E) Representative image of mouse dermis distant to the site of collagen and dextran injection. (F) Representative image of mouse dermis 24 h after injection of fluorescently labeled collagen. (G) Primary fibroblasts from wild-type or littermate uPARAP-deficient mice (hatched bars) were allowed to internalize ^{125}I-labeled collagen for 5 h, after which the cells were trypsinized, washed, and reseeded. At 5 and 9 h after collagen exposure (0 and 4 h after reseeding), the cells (left) and the supernatant (right) were separated, and radioactivity in the TCA-precipitable fraction and the non-TCA–precipitable fraction was measured. Error bars indicate SDs. (H and I) Effect of systemic metalloproteinase inhibition on intracellular collagen degradation. (H) GM6001 treatment of mice inhibits MMP activity in vivo. Mice were treated with GM6001 or vehicle 24 and 0.5 h before i.p. injection with either the MMP-activated toxin PrAg-L1 or the nonactivatable control toxin PrAg-U7 (circles, vehicle + PrAg-L1 [n = 8]; squares, GM6001 + PrAg-L1 [n = 5]; triangles, vehicle + PrAg-U7 [n = 5]). *, P = 0.041, log-rank test. (I) Percentage of collagen-internalizing cells in the dermis of vehicle-treated or GM6001-treated mice. n = 3 for each group of collagen-injected mice treated with vehicle or with GM6001. *, P < 0.05, Student's t test, two tailed. The quantitative data in this and the following figures are shown as mean ± SD and were obtained by counting 40–120 cells per z stack from four to six serial z stacks per mouse. (J) Percentage of collagen-internalizing cells in the dermis of mice injected with wild-type (wt) collagen or collagenase-resistant (*Col1a1*$^{r/r}$) collagen. n = 4 for each group of collagen-injected mice. *, P < 0.01, Student's t test, two tailed. Bars: (A) 50 µm; (B–D) 10 µm; (E and F) 15 µm.

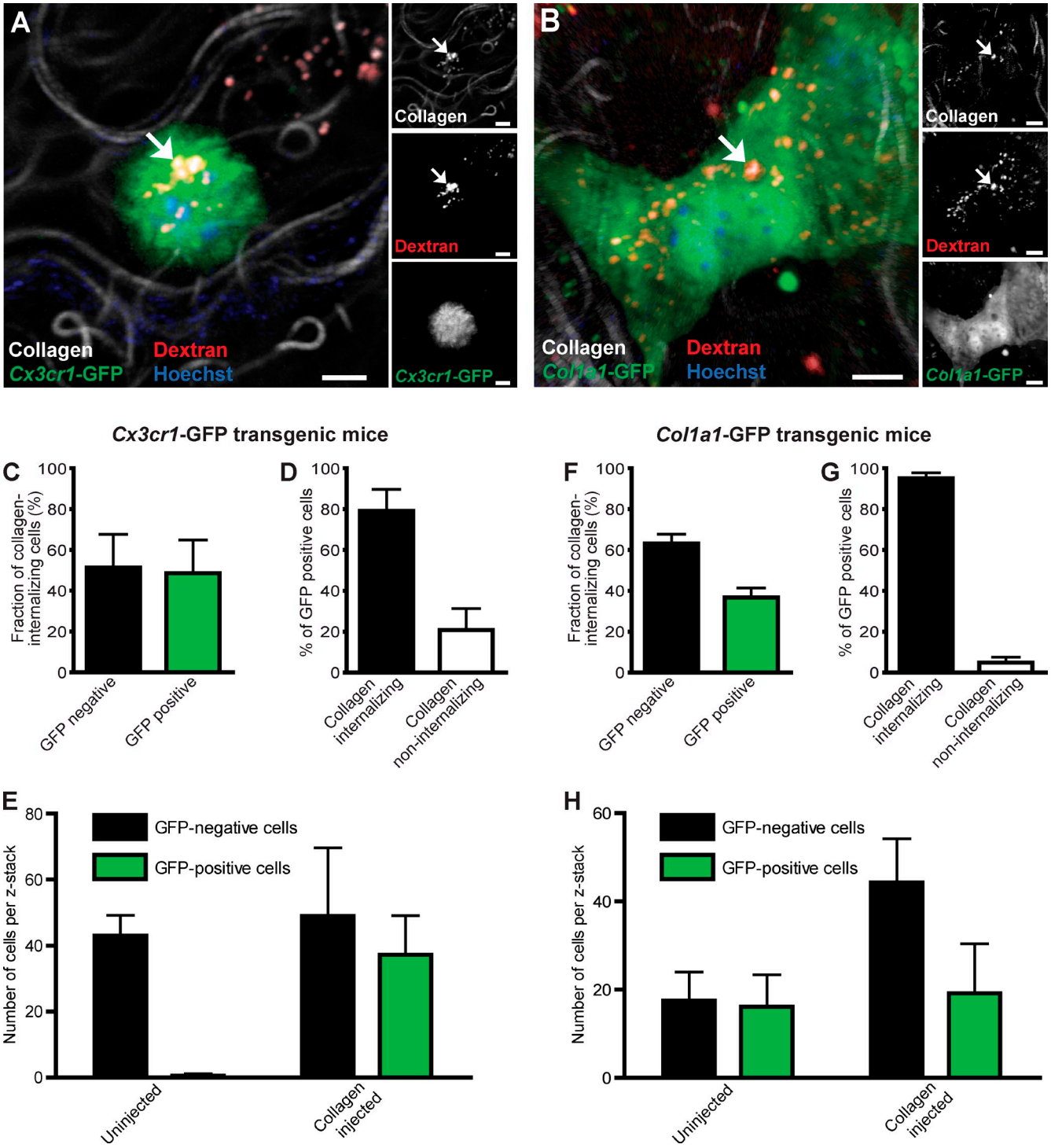

Figure 3. **Macrophages and fibroblasts mediate intracellular collagen degradation in vivo.** (A) High magnification image of the dermis of a collagen-injected *Cx3cr1*-GFP transgenic mouse. Example of endocytic vesicle containing collagen and Texas red dextran shown with arrows in a GFP-positive cell demonstrates intracellular collagen degradation by macrophages. (B) Representative high-magnification image of the dermis of a collagen-injected *Col1a1*-GFP transgenic mouse (GFP-tagged fibroblasts). Example of endocytic vesicle containing collagen and Texas red dextran shown with arrows in a GFP-positive cell demonstrates intracellular collagen degradation by fibroblasts. Bars: (A) 10 µm; (B) 5 µm. (C) Percentage of cells internalizing collagen that are GFP negative and GFP positive in collagen-injected *Cx3cr1*-GFP transgenic mice. (D) Percentage of *Cx3cr1*-GFP–positive cells displaying or not displaying intracellular collagen. $n = 4$ for collagen-injected *Cx3cr1*-GFP mice. (E) Cell counts in noninjected or collagen-injected dermis, as determined by the counting of *Cx3cr1*-GFP–positive and GFP-negative cells in z stacks from the injection field. $n = 5$ for uninjected mice, and $n = 4$ for collagen-injected mice. (F) Percentage of cells internalizing collagen that are GFP negative and GFP positive in collagen-injected *Col1a1*-GFP transgenic mice. (G) Percentage of GFP-positive cells displaying or not displaying intracellular collagen. $n = 4$ for collagen-injected *Col1a1*-GFP mice. (H) Cell counts in noninjected or collagen-injected dermis, as determined by the counting of *Col1a1*-GFP–positive and GFP-negative cells in z stacks from the injection field. $n = 3$ for uninjected mice, and $n = 3$ for collagen-injected mice. Data are shown as means ± SD.

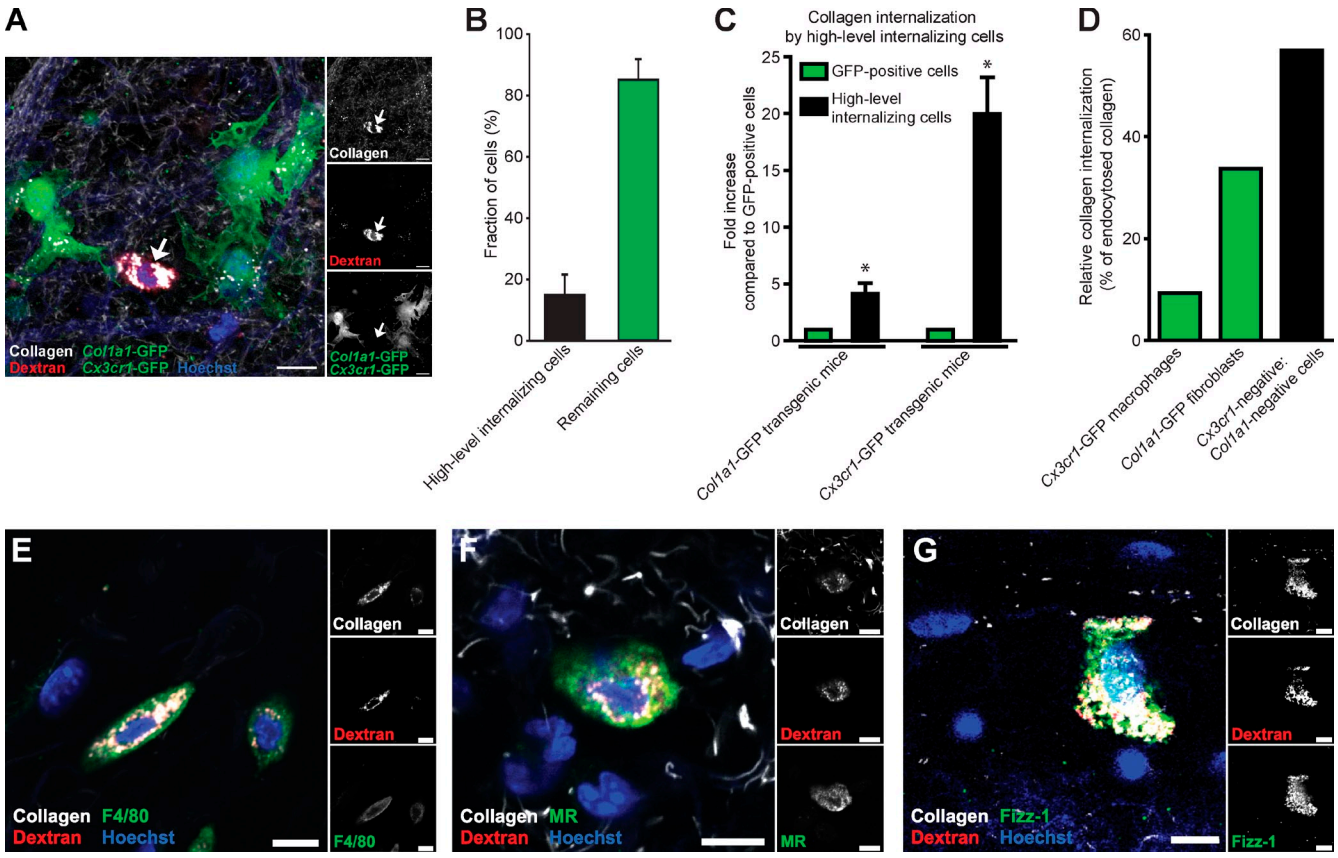

Figure 4. **High-level collagen-internalizing cells are M2-like macrophages.** (A) Representative image of the dermis from collagen-injected *Cx3cr1*-GFP;*Col1a1*-GFP double-transgenic mice. Note the presence of a high-level collagen-internalizing cell that is GFP negative (arrows). Bars, 20 µm. (B) Percentage of cells belonging to the high-level internalizing cell population. Data are expressed as means ± SD and were obtained by counting cells in four to six serial z stacks per mouse. $n = 5$. (C) Image-based analysis of collagen uptake in cells belonging to the high-internalizing cell population compared with *Col1a1*-GFP–positive cells or compared with *Cx3cr1*-GFP–positive cells. Data are expressed as mean fold increases ± SD and were obtained by measuring relative fluorescence intensity in 6–15 high-level internalizing cells per mouse and comparing with collagen internalization by GFP-positive cells present in the same sections. $n = 4$ for *Col1a1*-GFP mice and *Cx3cr1*-GFP mice. *, $P < 0.05$, Wilcoxon rank-sum test, two tailed. (D) Relative collagen internalization by *Cx3cr*-GFP–positive cells and *Col1a1*-GFP–positive cells and by high-level internalizing GFP-negative cells. The graph was generated by combining the measured fold differences in collagen uptake ($n = 4$ mice, 3–4 z stacks per mouse) and the determined fractions of the different cell types ($n = 4$–5 mice for each analysis, 4–6 z stacks per mouse). (E–G) 20 h after collagen injection into wild-type mice, the dermis was whole-mount stained for F4/80 (E), MR (F), and Fizz1 (G). Bars, 10 µm.

computer-assisted image analysis showed that collagen accumulation by this cell population was, respectively, 4 and 20 times higher than the total collagen accumulation in *Col1a1*-GFP–positive fibroblasts and *Cx3cr1*-GFP–positive macrophages (Fig. 4 C). Indeed, although low in abundance, this cell population accounted for 57% of all intracellularly located collagen (Fig. 4 D). We hypothesized that these vigorously collagen-internalizing cells represented a subpopulation of macrophages that were *Cx3cr1*-GFP negative. In support of this, whole-mount staining showed that 27 out of 27 identified high-level internalizing cells were positive for the macrophage marker F4/80 (Fig. 4 E).

Activated macrophages traditionally have been classified into two main populations, designated M1 and M2. M1-polarized macrophages principally serve as immune effectors, whereas M2-polarized macrophages engage in various tissue-remodeling processes, including wound repair (Mosser and Edwards, 2008) and tumor invasion (Sica et al., 2008; Wang and Joyce, 2010). Interestingly, whole-mount immunostaining of collagen-injected dermis showed that the vigorously collagen internalizing *Cx3cr1*-GFP–negative macrophages expressed both MR and Fizz1, two established markers for M2 polarization (Fig. 4, F and G), suggesting that macrophages with an M2-polarized phenotype may have a key role in dermal collagen degradation. To further explore the potential contribution of M2-like macrophages to intracellular collagen degradation, we next isolated human peripheral blood monocytes and derived, respectively, M1-polarized (by exposure to granulocyte–macrophage colony-stimulating factor [GM-CSF], IFN-γ, and lipopolysaccharide) and M2-polarized (by exposure to macrophage colony-stimulating factor [M-CSF] and IL-4) macrophages. Consistent with a function in collagen turnover, cultured M2-polarized macrophages displayed internalization of radiolabeled rat tail tendon type I collagen at a 2.5-fold higher rate than M1-polarized macrophages (see Fig. 7 F).

MR and uPARAP are critical for macrophage-mediated intracellular collagen degradation in vivo

The aforementioned studies identified three distinct cell populations engaging in intracellular collagen degradation in vivo:

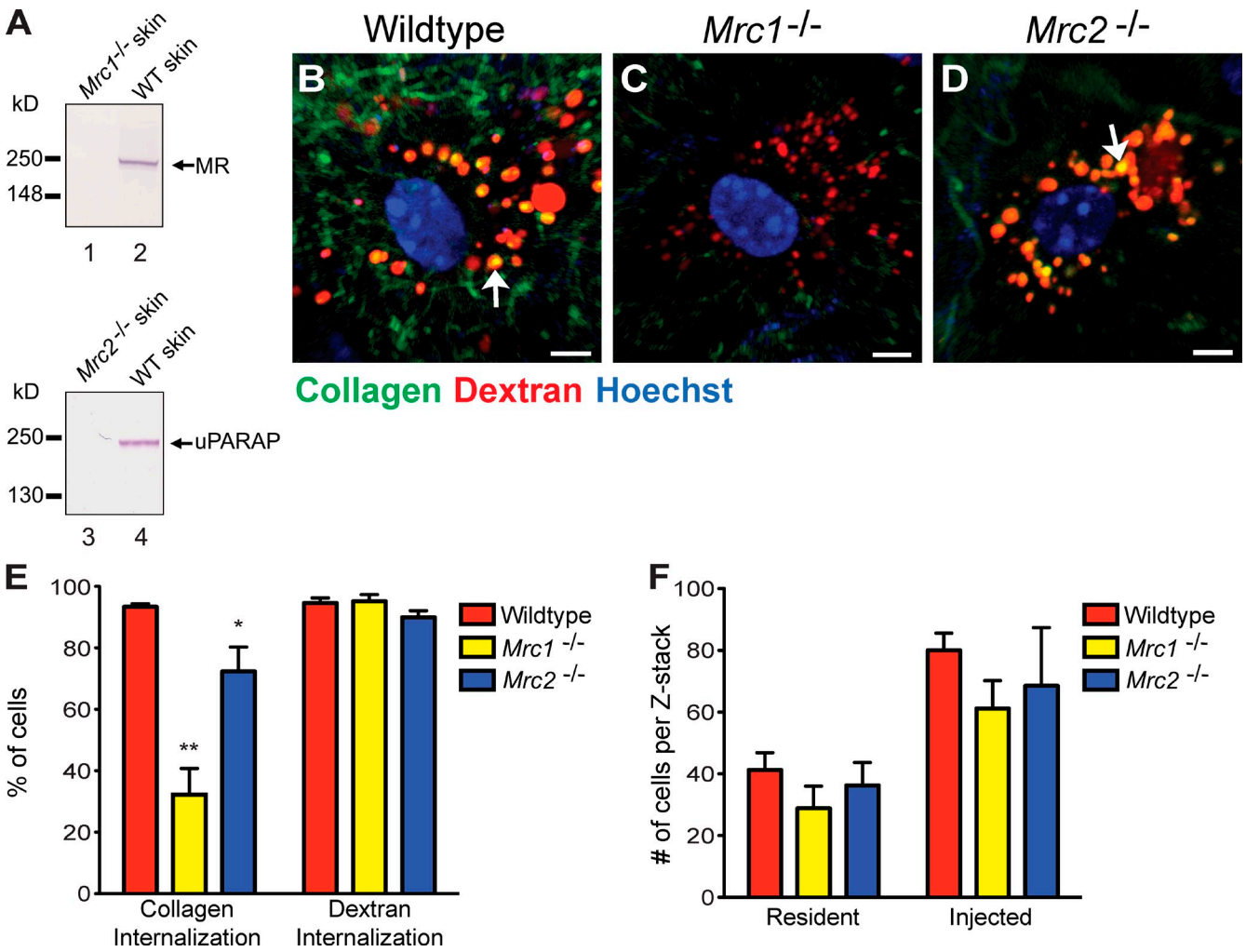

Figure 5. **MR and uPARAP facilitate intracellular collagen degradation in vivo.** (A) Western blot of MR (lanes 1 and 2) and uPARAP (lanes 3 and 4) in protein extracts from dermis of MR-deficient (*Mrc1*$^{-/-}$; lane 1) and a wild-type (WT) littermate (lane 2) or uPARAP-deficient (*Mrc2*$^{-/-}$; lane 3) and a wild-type littermate (lane 4). Arrows on the right show the positions of MR and uPARAP. Positions of molecular mass markers (kilodaltons) are indicated on the left. Specificity of MR and uPARAP detection is shown by the absence of immunoreactivity in *Mrc1*$^{-/-}$ and *Mrc2*$^{-/-}$ mice, respectively. (B–D) Representative examples of collagen uptake in cells from the dermis of wild-type (B), *Mrc1*$^{-/-}$ (C), and *Mrc2*$^{-/-}$ (D) mice 24 h after collagen injection. Bars, 10 µm. Arrows in B and D show examples of collagen in lysosomal vesicles. (E) Percentage of cells in collagen- and dextran-injected wild-type ($n = 5$), *Mrc1*$^{-/-}$ ($n = 3$), and *Mrc2*$^{-/-}$ ($n = 5$) dermis that internalize collagen or dextran. *, $P < 0.05$; and **, $P < 0.01$ relative to collagen-internalizing cells in wild-type mice (Student's *t* test, two tailed). (F) Enumeration of cells present in noninjected or collagen-injected dermis of wild-type ($n = 3$), *Mrc1*$^{-/-}$ ($n = 3$), and *Mrc2*$^{-/-}$ ($n = 3$) mice. Error bars show means ± SD.

Cx3cr1-GFP–positive macrophages and *Col1a1*-GFP–positive fibroblasts, both displaying low collagen-internalizing capacity, and M2-like macrophages, which display high collagen-internalizing capacity. We next set out to identify the specific receptors mediating collagen uptake by each of the three cell populations. Western blots of proteins extracted from injection fields 24 h after collagen injection showed expression of both MR and uPARAP by cells present in the injected area (Fig. 5 A), suggesting a potential role of the two collagen receptors in cellular collagen uptake in vivo. Therefore, we first explored the overall contribution of the two receptors to intracellular collagen degradation by quantifying the cellular uptake of collagen in MR- and uPARAP-deficient mice (Fig. 5, B–E). Interestingly, loss of MR was associated with a dramatic 60% decrease in the fraction of cells internalizing collagen (Fig. 5, C and E, left bars). Importantly, loss of MR was not associated with a general loss of endocytic capacity, as the fraction of cells internalizing fluorescent dextran was similar in MR-deficient and littermate wild-type mice (Fig. 5 E, right bars). Likewise, the total number of cells present in the injection field before and after collagen injection was unaffected by MR deficiency (Fig. 5 F). A smaller, but significant (21%), decrease in the fraction of cells internalizing collagen was observed in uPARAP-deficient mice (Fig. 5 E, left bars). As was the case for MR deficiency, this internalization defect was specific for collagen, as dextran internalization was unaffected by the loss of uPARAP (Fig. 5 E, right bars), as was the total number of cells residing in the dermis before and after collagen injection (Fig. 5 F). Collectively, these data directly demonstrate that both MR and uPARAP specifically contribute to cellular uptake of collagen in vivo.

To determine the specific cell populations displaying MR- and uPARAP-dependent collagen internalization in vivo,

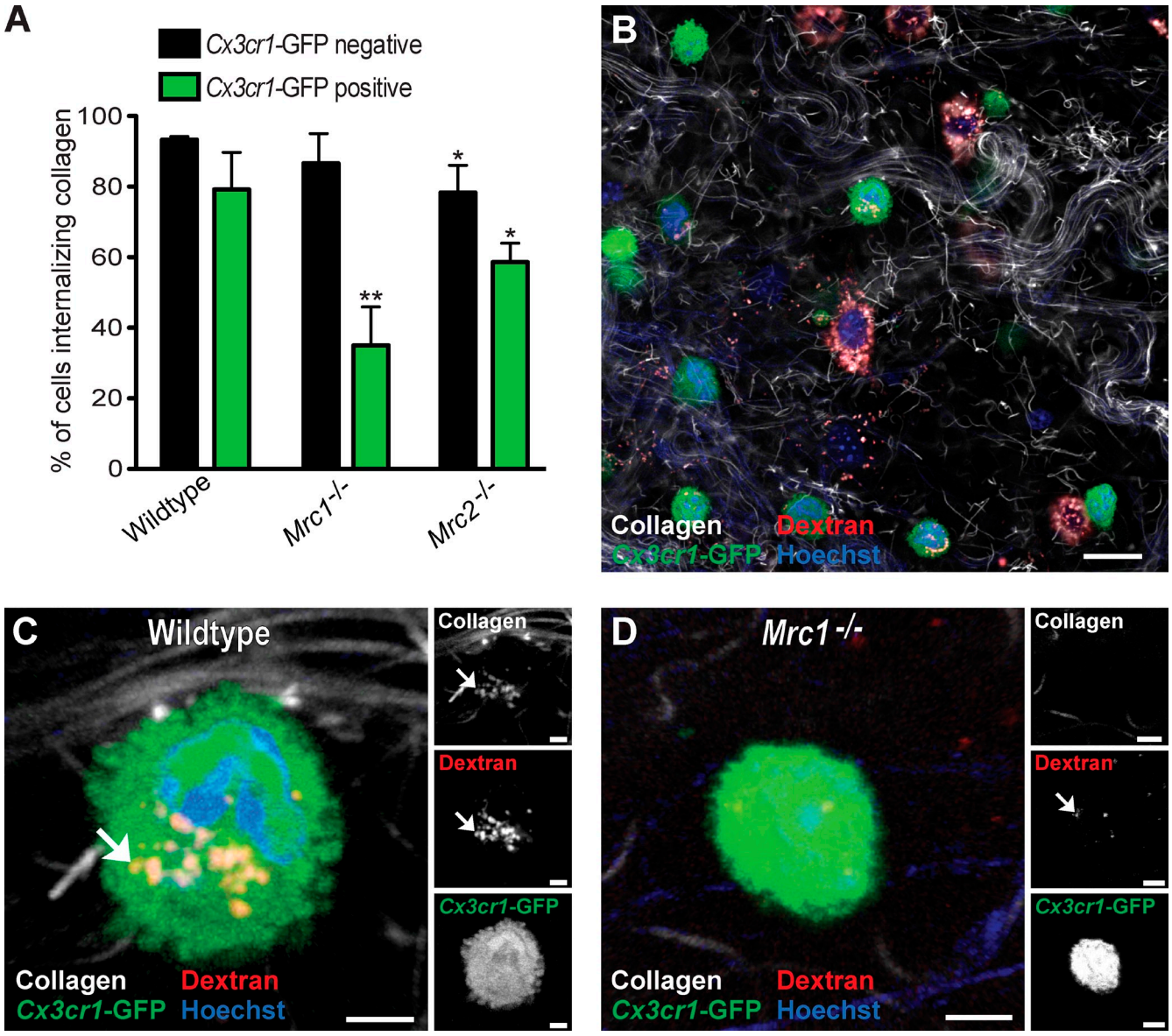

Figure 6. ***Cx3cr1*-GFP–expressing macrophages use both MR and uPARAP for the cellular uptake of collagen in vivo.** (A) Percentage of collagen-internalizing GFP-negative and GFP-positive cells from *Cx3cr1*-GFP transgenic mice that are *Mrc1*- and *Mrc2*-sufficient (referred to as wild type; $n = 4$), *Mrc1*$^{-/-}$ ($n = 4$), or *Mrc2*$^{-/-}$ ($n = 4$) mice. All mice were injected with fluorescent collagen. *, $P < 0.05$; and **, $P < 0.01$ relative to wild-type *Cx3cr1*-GFP transgenic mice (Student's *t* test, two tailed). Error bars show means ± SD. (B–D) Representative low-magnification image of the dermis of a collagen-injected *Cx3cr1*-GFP transgenic wild-type mouse (B) and representative high-magnification image of the dermis of collagen-injected *Cx3cr1*-GFP transgenic wild-type mice (C) and *Mrc1*$^{-/-}$ mice (D). Arrows show examples of internalized collagen. Bars: (B) 50 µm; (C) 10 µm; (D) 8 µm.

we next interbred *Cx3cr1*-GFP mice with MR- and uPARAP-deficient mice to generate *Cx3cr1*-GFP transgenic mice lacking either MR or uPARAP. These mice then were injected with fluorescent collagen, dextran, and Hoechst dye, and the fraction of GFP-positive and -negative cells that internalized collagen in the presence and absence of MR and uPARAP was determined (Fig. 6, A, B [representative examples of injection field], C [GFP-positive and MR wild-type cell], and D [GFP-positive and MR-deficient cell]). Loss of MR reduced the fraction of GFP-positive cells that internalized collagen from 79 to 35%, revealing that MR mediates cellular collagen uptake by *Cx3cr1*-GFP–positive macrophages in vivo. Loss of uPARAP resulted in a smaller, but significant ($P < 0.05$), reduction in the number of GFP-positive cells that internalized collagen from 79 to 59%, revealing a similar role for uPARAP in cellular collagen uptake by *Cx3cr1*-GFP–positive macrophages. Importantly, loss of MR also resulted in a dramatic diminution of the capacity of M2-like dermal macrophages to endocytose collagen, with the majority of MR-deficient M2-like macrophages displaying low or no collagen uptake (Fig. 7, A–C). In contrast to the *Cx3cr1*-GFP macrophages, uPARAP deficiency had no effect on collagen internalization by this subset of macrophages (Fig. 7 D). Consistent with this finding, in vitro differentiation of human monocytes to M2-polarized macrophages led to a marked up-regulation of MR (Fig. 7 E), and treatment of M2-polarized macrophages with MR antibodies dramatically reduced their capacity to internalize

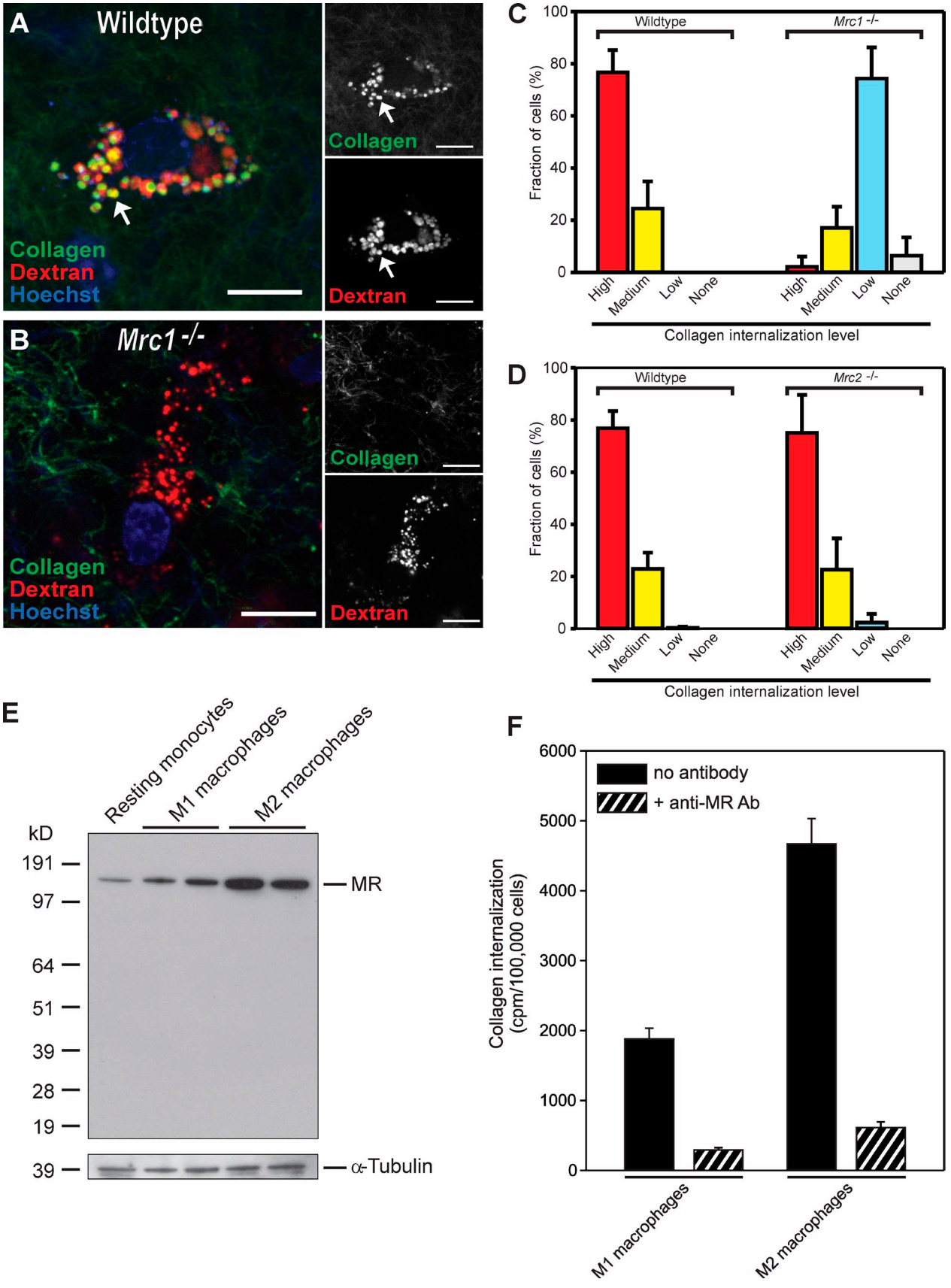

Figure 7. **MR-dependent collagen internalization by M2-like macrophages.** (A and B) Representative high-magnification image of a high-level internalizing cell of the dermis of wild-type (A) and *Mrc1*$^{-/-}$ mice (B). Examples of endocytic vesicle containing collagen and dextran are indicated with arrows. No or very little collagen is observed in endocytic vesicles in the *Mrc1*$^{-/-}$ mice (compare A and B). Bars, 10 µm. (C and D) In wild type (C and D, left four

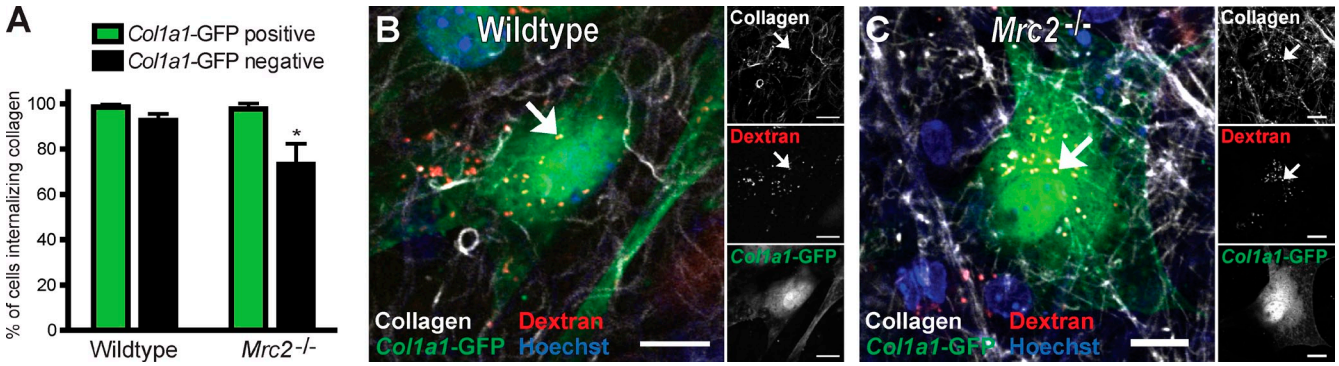

Figure 8. **Fibroblasts internalize collagen independently of uPARAP in vivo.** (A) Percentage of collagen-internalizing GFP-positive and GFP-negative cells in the dermis of collagen- and dextran-injected *Mrc2*$^{+/+}$ (wild type; $n = 4$) and *Mrc2*$^{-/-}$ ($n = 6$) mice. *, $P < 0.01$, Student's *t* test, two tailed. Data are shown as means ± SD. (B and C) Representative high-magnification images of the dermis of collagen-injected *Col1a1*-GFP transgenic *Mrc2*$^{+/+}$ (B) and *Col1a1*-GFP transgenic *Mrc2*$^{-/-}$ (C) mice. Examples of endocytic vesicles containing collagen and dextran are indicated with arrows. Bars, 10 µm.

radiolabeled rat tail tendon collagen (Fig. 7 F). Collectively, these data show that the acquisition of MR expression during M2 polarization specifically endows these macrophages with the capacity to efficiently internalize and degrade collagen.

Col1a1-GFP–positive fibroblasts internalize collagen independent of uPARAP in vivo

Dermal fibroblasts explanted in primary culture internalize collagen in a strictly uPARAP-dependent manner (East et al., 2003; Engelholm et al., 2003; Madsen et al., 2007). Because ≥37% of the cells internalizing collagen in the injection fields could be identified as fibroblasts, we next queried the specific role of uPARAP in collagen uptake by fibroblasts in vivo. *Col1a1*-GFP transgenic mice were interbred with uPARAP-deficient mice to generate uPARAP-sufficient and -deficient GFP-tagged *Col1a1* transgenic mice that were injected with fluorescent collagen, dextran, and Hoechst dye and analyzed for collagen internalization. Surprisingly, loss of uPARAP did not result in a reduction of number of GFP-positive cells internalizing collagen, with >95% of the GFP-positive cells internalizing collagen in both uPARAP-deficient and -sufficient mice (Fig. 8, A–C), suggesting that other receptors govern cellular collagen uptake in this context.

Discussion

The extracellular machinery that executes the initial steps of interstitial and basement membrane collagen cleavage, which results in the formation of smaller partially denatured and degraded collagen fragments, is now well characterized. However, the subsequent fate of these collagenase digestion products has been less clear, in particular, regarding the specific events and molecules that lead to their possible cellular uptake and complete degradation into free amino acids within the lysosome (Rowe and Weiss, 2009; Bugge and Behrendt, 2011). In this study, we therefore developed a novel assay to visualize the cellular uptake of collagen and its trafficking to the lysosomes in vivo by exploiting the observation that acid-extracted fluorescently labeled collagen fibrils rapidly form collagen fiber networks when placed into the subcutaneous space and that the presence of this exogenous collagen, combined with the inoculation trauma, induced an active matrix catabolic environment. This novel assay allowed us to critically challenge several hypotheses that have emerged over the past several decades regarding intracellular collagen degradation and to directly query the contribution of specific cell types and cellular collagen receptors to the process in an in vivo setting.

A first important observation made was that collagen within the subcutaneous space is indeed efficiently endocytosed and routed to the lysosomal compartment. Thus, the majority of cells within dermal injection fields displayed collagen-containing lysosomes within 24 h after collagen injection. This adds strong support to the notion that the intracellular collagen observed in numerous electron microscopy studies (see Introduction) originates from the extracellular matrix and does not represent misfolded collagen rerouted for lysosomal degradation as previously proposed (Bienkowski et al., 1978; Berg et al., 1980). Our study, thus, definitively establishes intracellular collagen degradation as a physiologically relevant pathway for collagen turnover in vivo. Expression analysis revealed that cells within the injection field produced a variety of proteases with collagenolytic and gelatinolytic activity. Inhibition of metalloproteinase activity, including collagenase and gelatinase activity, had a modest, though significant, effect on cellular collagen uptake. A similar reduction in internalization of collagenase-resistant collagen compared with wild-type collagen was observed, suggesting that a significant fraction of the introduced collagen

bars), littermate *Mrc1*$^{-/-}$ mice (C, right four bars), or littermate *Mrc2*$^{-/-}$ mice (D, right four bars), the high-level internalizing cells were identified based on their prominent lysosomes and scored for the level of collagen uptake (high, medium, low, or none). $n = 4$ each for wild type, *Mrc1*$^{-/-}$ mice, and *Mrc2*$^{-/-}$ mice. (E and F) High-level MR-dependent collagen internalization by M2-like macrophages is recapitulated in vitro. Lysates from human blood monocytes differentiated in vitro to resting macrophages or stimulated to acquire an M1- or M2-polarized phenotype were analyzed by Western blotting for the expression of MR (E). The position of MR is indicated on the right. Positions of molecular mass markers (kilodaltons) are indicated on the left. (F) ^{125}I-labeled collagen was added to in vitro–generated M1- and M2-polarized macrophages. After 4 h, the intracellular fraction of each cell sample was isolated, and the amount of internalized collagen was measured. Ab, antibody. Data are shown as means ± SD.

is internalized only after initial MMP-mediated cleavage. Although, importantly, these observations do support a role of collagenases and fragmenting of collagen before its cellular uptake in vivo, the assay, as designed, likely understates the importance of these enzymes in facilitating intracellular degradation of endogenous collagen fibers. Thus, the exogenously introduced collagen is likely to form collagen networks that are overall less highly organized, less extensively cross-linked, and frequently partially denatured. These networks, therefore, in part, may resemble the products of collagenase-digested or trauma-denatured interstitial collagen and, thus, may display a physical state amenable to cellular uptake with limited or no further need for prior proteolytic modification by MMPs. Additionally, a fraction of the introduced collagen could fail to incorporate into any insoluble structures and instead be recognized and internalized in a soluble state. Altogether, we speculate that the internalization and intracellular degradation of endogenous fibrillar collagen might require even more proteolytic processing before internalization and therefore occur at a slower rate than what we observe for the exogenous fluorescently labeled collagen but otherwise involve the same receptors and cell types as identified in this study.

Using mice with cell lineage–specific fluorescent tags as well as in situ staining for cell lineage–specific markers, we identified three distinct cell populations engaging in intracellular collagen degradation in vivo: *Col1a1*-positive fibroblasts, a *Cx3cr1*-positive macrophage subpopulation, and M2-like macrophages. *Col1a1*-positive fibroblasts and *Cx3cr1*-positive macrophages contributed modestly to intracellular collagen turnover, whereas M2-like macrophages represented the principal cell type responsible for collagen turnover within this specific context. These inferred differences in the contribution to collagen turnover, however, are predicated on the assumption that the level of intracellular collagen observed reflects the rate of collagen internalization and is not, or only to a small degree, influenced by differences in lysosomal degradation rates between the three cell populations. However, because of the high abundance and large size of lysosomes in M2-polarized macrophages, we speculate that our study likely may underestimate, rather than overestimate, the overall contribution of M2-polarized macrophages to collagen turnover.

M2-polarized macrophages are a distinct subpopulation of macrophages that produce minimal amounts of inflammatory cytokines, oxygen, and nitrogen radicals and are inefficient in pathogen eradication (Mosser and Edwards, 2008). Rather, this macrophage subpopulation stimulates the synthesis of various extracellular matrix components through polyamine production and by the release of specific cytokines and therefore has been proposed to play a primary physiological role in promoting tissue repair. The current study lends important additional support to this hypothesis by showing that M2 polarization dramatically enhances the capacity to turnover extracellular matrix by an intracellular pathway in vivo. Importantly, intracellular collagen degradation by tumor-associated M2 macrophages could contribute to the promotion of tumorigenesis by this cell type, and therapeutic interference with this degradation pathway could form the basis for future antimetastatic treatment. Additional studies will be required to determine whether the collagen-degrading M2-like macrophage identified in this study represents a phenotypic subpopulation of these macrophages or whether the capacity to efficiently degrade collagen is inherent to all M2-polarized macrophages. Furthermore, it would be interesting to explore whether collagen uptake by M2-polarized macrophages by itself stimulates the capacity of this cell type to promote extracellular matrix deposition, thereby providing a mechanistic link between matrix degradation and synthesis.

MR and uPARAP are critical to cellular collagen uptake and degradation by a variety of mesenchymal cell types when cultured ex vivo and have emerged as candidate in vivo collagen internalization receptors within the last decade (Bugge and Behrendt, 2011). By quantitative studies of mice deficient in MR and uPARAP, we now were able to directly establish a role of both endocytic receptors in cellular collagen uptake and degradation in vivo. Thus, the absence of MR or uPARAP markedly reduced the fraction of cells that were capable of internalizing collagen. This internalization defect was specific to collagen, as shown by the unabated uptake of dextran by both MR- and uPARAP-deficient cells. In line with this finding, several prior ex vivo studies have demonstrated that the two receptors are not part of the general endocytic machinery but rather are highly selective for collagen and its degradation products as well as for a few other ligands (Ezekowitz et al., 1991; Otter et al., 1992; Prigozy et al., 1997; Tan et al., 1997; Lee et al., 2002; Royer et al., 2010; Paveley et al., 2011). The direct demonstration of the participation of MR or uPARAP in intracellular collagen degradation in vivo provides additional strong evidence that the phenotypic consequences of ablation of the two receptors, on skeletal and lung development, tissue fibrosis, and tumor invasion, are attributable in whole or in part to impaired collagen turnover (Curino et al., 2005; Malovic et al., 2007; Wagenaar-Miller et al., 2007; Wienke et al., 2007; Fasquelle et al., 2009; Bundesmann et al., 2012; López-Guisa et al., 2012; Madsen et al., 2012).

By imposing MR and uPARAP deficiency on mice carrying macrophage- and fibroblast-specific fluorescent tags, we were able to also query which cell types use the two receptors for collagen uptake. The finding that MR plays a critical role in collagen uptake by *Cx3cr1*-GFP–positive macrophages and M2-like macrophages in vivo is compatible with the expression of the receptor on macrophages and with previous studies showing that inhibition of MR by function-blocking antibodies or by gene ablation prevents ex vivo collagen uptake by, respectively, cultured human peripheral monocyte-derived macrophages and mouse peritoneal macrophages (Jürgensen et al., 2011; Madsen et al., 2011). The contribution provided by uPARAP to macrophage-mediated collagen uptake was also not a complete surprise, in the light of previous studies of uPARAP expression by macrophage subsets (Sheikh et al., 2000; Schnack Nielsen et al., 2002). Wholly unanticipated, however, was the seemingly complete independence of dermal fibroblasts on uPARAP for cellular collagen uptake in vivo, despite several previous studies demonstrating a strict uPARAP dependence of collagen uptake by primary mouse dermal fibroblasts, immortalized mouse embryonic fibroblasts, immortalized human gingival fibroblasts, and human fibrosarcomas when cultured ex vivo (East et al., 2003;

Engelholm et al., 2003; Madsen et al., 2011). The finding serves to underscore the dramatic phenotypic changes that may be imposed on cells by even brief ex vivo culture. It is important to stress, however, that our data in no way exclude that fibroblasts may both use and be dependent of uPARAP for collagen internalization in other contexts, such as lung development, protection from fibrosis, and tumor progression (Curino et al., 2005; Bundesmann et al., 2012; López-Guisa et al., 2012; Madsen et al., 2012). The natural question arising from the aforementioned discovery is which receptors are specifically responsible for the uPARAP-independent collagen internalization by dermal fibroblasts in vivo? Possible candidates are the collagen binding $\alpha1\beta1$ and $\alpha2\beta1$ integrins, which are expressed by fibroblasts, but this may be difficult to test as a result of the detrimental effects on cell adhesion and cell behavior that the genetic ablation or functional inhibition of these integrins is likely to impose (Fässler and Meyer, 1995; Stephens et al., 1995; Arora et al., 2000; Segal et al., 2001). In summary, our study definitively establishes intracellular collagen degradation as a physiologically relevant collagen internalization pathway in vivo, it suggests that dermal collagen is predominantly degraded by a quantitatively minor population of M2-like macrophages with additional contributions by *Cx3cr1*-GFP–positive macrophages and *Col1a1*-GFP–positive fibroblasts, and it directly establishes a key role of MR and uPARAP in this process.

Materials and methods

Animal experiments

All procedures involving live animals were performed in an Association for Assessment and Accreditation of Laboratory Animals Care International–accredited vivarium following institutional guidelines and standard operating procedures. Genotyping for the *Mrc1* endogenous and targeted allele was performed with the primers MR forward, 5′-GACCTTGGACTGAGCAAAGGGG-3′, and MR reverse, 5′-GACATGATGTCCTCAGGAGGACG-3′ (Lee et al., 2002). Genotyping for the *Mrc2* endogenous allele was performed with the primers Exon3-5′, 5′-TCTACACCATCCAGGGAAACTCAC-3′, and Exon3-3′, 5′-TTAAACTGGTAACAGCTGTCAGTC-3′. The *Mrc2*-targeted allele was amplified using the primers targ1, 5′-TCCTACAAATACACGCTGGCGATA-3′, and targ2, 5′-GCAGTTCCCTTTTAAATGCAAATCA-3′ (Engelholm et al., 2003). *B6.129P-Cx3cr1*$^{tm1Litt/J/+}$ mice (Jung et al., 2000) were obtained from The Jackson Laboratory and interbred with mice carrying targeted uPARAP/Endo180 alleles in an FVB/N background or MR alleles in a C57BL/6J background. Genotyping for the *Cx3cr1* endogenous allele was performed with the primers E3 3′, 5′-TTCACGTTCGGTCTGGTGGG-3′, and E3 5′, 5′-GGTTCCTAGTGGAGCTAGGG-3′. The GFP-targeted allele was amplified with T3 3′, 5′-GATCACTCTCGGCATGGACG-3′, and the same reverse primer as in the endogenous amplification. *Col1a1*$^{GPF/0}$ transgenic mice, which express enhanced GFP under the *Col1a1* promoter, have been previously described (Krempen et al., 1999). Expression of GFP by the *Col1a1*$^{GPF/0}$ transgenic mice was determined by illuminating the mice with the blue light of a NightSea DFP-1 Dual Fluorescent Protein Flashlight (Fun-In Underwater Photo Equipment Co., Ltd.) using the appropriate filter goggles. *Col1a1*^{tm1Jae}/J mice (*Col1a1*$^{r/r}$; Liu et al., 1995) were obtained from The Jackson Laboratory. Genotyping for the endogenous allele was performed with the primers E38wt, 5′-GGACAACGTGGTGTGGTCGGTC-3′, and I43com, 5′-GCATGTCTGAAGAAGAGGTCT-3′. The targeted allele was amplified with the primer E38mut, 5′-GGACAACGTGGTGCCGCGGGTC-3′, and the same reverse primer as in the endogenous amplification.

Labeling of collagen with fluorescent dyes

Collagen labeling was performed by modification of a previously described procedure (Birkedal-Hansen et al., 2003). In brief, acid-extracted rat tail tendon type I collagen at 3 mg/ml in 13 mM HCl was neutralized and incubated for 2 h at 37°C to form a gel. The collagen gel was covalently labeled with Alexa Fluor 488, 594, or 647 fluorescent dye (Invitrogen) for 2 h at room temperature followed by 2 d of multiple washes in PBS, which removed nonbound dye and collagen incapable of forming fibrils after the labeling. The collagen was then redissolved in 13 mM HCl. The ability of the labeled collagen to reform collagen fibers after neutralization was verified by fluorescence microscopy for assessment of proper fiber formation and for trypsin resistance by overnight incubation at 37°C with a 0.05% trypsin/EDTA solution. To study collagen type I with a mutation in the collagenase cleavage site, collagen fibers were dissected from the tails of *Col1a1*$^{r/r}$ mice or littermate wild-type mice. The collagen was separated from other tissue, such as blood vessels, under a dissecting microscope (Stemi 2000 Dissection Stereomicroscope; Carl Zeiss). Collagen was dried and dissolved in 0.5 M acetic acid at 4°C. To clarify the dissolved collagen, the solution was filtered through a 40-µm nylon membrane and centrifuged at 24,000 *g* at 4°C for 3 h. Finally, the collagen solution was dialyzed against 0.01 N HCl and fluorescently labeled as described in the previous paragraph.

In vivo collagen internalization assay

Mice were anesthetized by isoflurane inhalation, and under anesthesia, both flanks were shaved and injected subcutaneously with 60 µl of 0.4-mg/ml fluorescently labeled collagen and 0.3 mg/ml fluorescently labeled 10-kD Texas red dextran (Invitrogen) or with fluorescently labeled collagen alone. The solution was neutralized immediately before injection. 18–24 h later, mice were injected intravenously with 150 µl of 4-mg/ml Hoechst 33342 trihydrochloride trihydrate dye (Invitrogen). Mice were euthanized 4–6 h later, the dermal flanks were excised, and the tissue was immediately imaged by confocal microscopy. To determine the overall clearance rate of the injected fluorescently labeled collagen, mice were injected with Alexa Fluor 488–conjugated collagen, and after 4 h, 1 d, 2 d, 3 d, or 5 d, the mice were euthanized, and skins encompassing the injection site were excised. Each skin piece was cut into small fragments and incubated dermis-side down in a solution of 900 µl HBSS and 100 µl Liberase DH (Roche) at 37°C for 90 min. Subsequently, 250 µl of 1-M acetic acid was added, and the samples were incubated for an additional 60 min at 37°C. The samples were clarified by centrifugation at 400 *g* at 4°C for 10 min followed by centrifugation at 20,000 *g* at 4°C for 20 min. The extracted fluorescence was measured using a plate reader (Wallac 1420 Victor2; PerkinElmer).

Metalloproteinase inhibition

GM6001 (U.S. Biologicals) was formulated for in vivo administration as a 20-mg/ml slurry in 0.9% saline and 4% carboxymethylcellulose (Almholt et al., 2008). Recombinant protective antigen (PA)-L1, PA-U7, and FP59-AGG were generated in avirulent strains of *Bacillus anthracis* or *Escherichia coli* and purified by fast protein liquid chromatography (Liu et al., 2000). For toxin challenge, 8–10-wk-old C57BL/6J females (The Jackson Laboratory) were injected intraperitoneally with either 100 mg/kg GM6001 or vehicle at 24 and 0.5 h before toxin challenge. Mice were then injected intraperitoneally with MMP-activated anthrax toxin: 1.5 mg/kg PA-L1 and 0.5 mg/kg FP59-AGG. Mice were monitored hourly and were euthanized if moribund. For collagen internalization experiments, mice were injected with 100 mg/kg GM6001 24 and 0 h before collagen injection and 3 h before analysis.

Confocal microscopy

Confocal imaging was performed using an inverted confocal microscope (IX81; Olympus) equipped with a scanning head (FluoView 1000; Olympus). All of the images were acquired using a U Plan S Apochromat 60× numerical aperture 1.2 water immersion objective. Imaging was performed directly on fresh tissue and at room temperature. GFP and Alexa Fluor 488 were excited with a 488-nm laser (Olympus), Texas red and Alexa Fluor 594 were excited with a 561-nm laser (Showa Optronic), and Alexa Fluor 647 was excited with a 633-nm laser (Melles Griot). Image acquisition was performed using FluoView acquisition software (Olympus). For the z-stack acquisition, the starting focal plane was chosen at 15–20 µm from the surface of the dermis, and the z step was set at 2 µm.

Quantitative analysis of cellular collagen uptake

For quantification of collagen and dextran internalization, five z stacks of 29-µm sections were collected for each mouse, each stack at the same depth within the tissue. Z stack locations were chosen at random in the vicinity of the collagen injection site. Internalization was scored by the presence of fluorescently labeled collagen and/or dextran in perinuclear vesicular structures. Total number of cells in each z stack was determined by counting all nuclei stained with Hoechst dye and in the case of *Cx3cr1*-GFP or *Col1a1*-GFP transgenic mice scoring each cell as either GFP positive or GFP negative. Final values for cell numbers per mouse were the mean of four to six z stacks,

making up $n = 1$. The *Cx3cr1*-GFP–negative/*Col1a1*-GFP–negative high-level collagen-internalizing cell population could be identified based solely on the prominence of their lysosomal compartment. To evaluate collagen uptake by this cell population, each cell was scored 0–3: 0 = none (no collagen-positive vesicles), 1 = low (1–5 collagen-positive vesicles), 2 = medium (5–15 collagen-positive vesicles), and 3 = high (>15 collagen-positive vesicles). To determine the level of collagen uptake by the high-level internalizing cells, a comparison to *Cx3cr1*-GFP–positive or *Col1a1*-GFP–positive cells was made. Based on z stacks from each of these transgenic mice, the high-level internalizing cells were identified as described in the previous paragraph, and an outline of the high-level internalizing cells and of the GFP-positive cells was drawn using ImageJ software (National Institutes of Health) to generate the regions of interest. The threshold for the fluorescent collagen was selected to allow maximum detection of collagen-positive vesicles while minimizing the contribution from extracellular fibrillar collagen. For each region of interest, the raw integrated density values were used for calculating the relative collagen uptake by high-level internalizing cells compared with GFP-positive cells in the same plane. From each z stack, only slices with both GFP-positive cells and high-level internalizing cells present were used for the analysis, and a mean fold difference between the two cell populations was calculated. The total relative fold difference in collagen uptake was calculated based on the analysis of 42 GFP-positive cells and 45 GFP-negative high-level internalizing cells in four *Col1a1*-GFP transgenic mice and 56 GFP-positive cells and 43 GFP-negative high-level internalizing cells in four *Cx3cr1*-GFP transgenic mice (in both cases, three to four z stacks per mouse were analyzed). To calculate the amount of internalized collagen by *Cx3cr*-GFP–positive cells, *Col1a1*-GFP–positive cells, and high-level internalizing GFP-negative cells, the fold differences in collagen internalization were multiplied to the fraction of collagen-internalizing *Cx3cr1*-GFP–positive cells (48.6%), *Col1a1*-GFP–positive cells (36.8%), or high-level internalizing *Cx3cr1*-GFP–negative, *Col1a1*-GFP–negative, cells (14.9%).

Western blotting

Approximately 1 cm^2 of mouse skin was excised and homogenized in lysis buffer (50 mM Tris-HCl, pH 7.4, 150 mM NaCl, 1% Triton X-100, 0.5% Nonidet P-40, and 0.1% SDS with protease inhibitor cocktail [EMD Millipore]). Protein concentrations were determined using a bicinchoninic acid assay (Thermo Fisher Scientific), and 20 µg protein was used for Western blotting under nonreducing conditions. Western blotting against MR was performed using 2 µg/ml goat anti-MR antibody (clone MR5D3; AbD Serotec). Western blotting against uPARAP was performed with a solution containing 0.5 µg/ml monoclonal mouse anti-uPARAP antibody (clone 2h9F12; Sulek et al., 2007) mixed with alkaline phosphatase–conjugated secondary antibody. Anti-uPARAP antibody and the secondary antibody were mixed at a molar ratio of 3:1 and preincubated for 20 min to avoid the signal from endogenous mouse IgG. Protein lysates from M1 macrophages, M2 macrophages, and resting macrophages (generated as described in the section Ex vivo collagen internalization assay) were analyzed by Western blotting for the detection of MR and tubulin (loading control). Protein concentrations were determined, and equal protein amounts were loaded. The following primary antibodies were used: 2 µg/ml monoclonal mouse anti-MR antibody (BD) and monoclonal mouse anti-tubulin antibody (Santa Cruz Biotechnology, Inc.).

Gene expression analysis by real-time PCR

Gene expression was performed by real-time PCR in three tissue samples from collagen-injected or noninjected skin. In brief, 1 µg of total RNA was used for first-strand cDNA synthesis (Superscript III First-Strand Synthesis SuperMix; Invitrogen). The real-time PCR detection system (iCycler iQ; Bio-Rad Laboratories) and iQ SYBR Green Supermix (Bio-Rad Laboratories) were used for analysis. In brief, the reaction mixture contained 500 ng cDNA, housekeeping gene primers, and gene-specific forward and reverse primers for each gene at a final concentration of 1 µM. The real-time cycler conditions were as follows: PCR initial activation step at 95°C for 3 min, 40 cycles each of denaturing at 95°C for 15 s, and annealing/extension at 60°C for 1 min followed by a melting curve analysis of 55–95°C with 0.5°C increment, 5 s per step. A negative control without a template was included to assess the overall specificity of the reaction. The comparative cycle threshold ($\Delta\Delta C_T$) method was used to achieve the relative fold changes in gene expression between noninjected and collagen-injected skin. Primers are shown in Table S1.

Whole-mount staining

Whole-mount staining was performed 24 h after collagen and dextran injection. Skin was fixed for 4 h (MR and Fizz1 staining) or 16 h (F4/80 staining), and for the MR and Fizz1 staining, the skin was subsequently permeabilized by incubation in 1% Triton X-100 in PBS for 45 min. The skin was washed in PBS + 0.5% BSA + 0.2% Triton X-100 (PBS-BT), blocked in PBS-BT + 2% goat serum for ≥1 h, and incubated overnight at 4°C with primary antibody diluted in PBS-BT + 2% goat serum at the following ratios: rat anti-F4/80 (clone BM8, eBioscience) diluted 1:200, rat anti-MR (AbD Serotec) diluted 1:200, and rabbit anti-Fizz1 (PeproTech) diluted 1:400. Tissues were washed thoroughly in PBS-BT and incubated overnight at 4°C with Alexa Fluor 488–conjugated secondary antibodies diluted 1:500 in PBS-BT. After washing in PBS-BT, the tissue was incubated for 1 h with Hoechst diluted 1:10,000 in PBS-BT, and after subsequent washing, the skin was imaged as described in the "Confocal microscopy" section.

Ex vivo collagen internalization assay

Human monocytes were isolated from healthy donors as previously described (Jürgensen et al., 2011). In brief, mononuclear cells were isolated from whole blood using density gradient centrifugation (Lymphoprep; Axis-Shield). After this, monocytes were isolated using an automated cell isolator (RoboSep; StemCell Technologies, Inc.) and CD14 selection kit (EasySep Human Buffy Coat; StemCell Technologies, Inc.). The monocytes were differentiated in AIM-V media (Invitrogen) supplemented with the following specific cytokines: M1 macrophages, 5 ng/ml recombinant human GM-CSF (Sigma-Aldrich) for 7 d followed by 5 ng/ml recombinant human GM-CSF, 5 ng/ml recombinant human IFN-γ (R&D Systems), and 100 ng/ml lipopolysaccharide (Sigma-Aldrich) for 2 d; M2 macrophages, 20 ng/ml recombinant human M-CSF and 12.5 ng/ml recombinant human IL-4 (both obtained from R&D systems) for 9 d; and resting macrophages were generated by culturing for 9 d without cytokines. Collagen internalization assay was performed essentially as previously described (Jürgensen et al., 2011). In brief, macrophages were incubated in AIM-V medium supplemented with 1.5% BSA, 20 mM Hepes, and 10 µM of the cysteine protease inhibitor E64d (Merck Biosciences) for 30 min. ^{125}I-labeled rat tail collagen I was added to a concentration of 150 ng/ml, and after a 4-h incubation at 37°C, the intracellular fraction was isolated and measured using a γ counter. M1 and M2 macrophages were evaluated for their ability to internalize collagen in the presence or absence of a function-blocking anti-MR antibody (10 µg/ml; R&D Systems). All samples were analyzed in triplicates. Fibroblasts from the skin of newborn *Mrc2*$^{-/-}$ mice or wild-type littermates were isolated by trypsinization overnight at 4°C as previously described (Engelholm et al., 2003). One million cells were seeded in 6-well plates in duplicates in DMEM with 10% FCS and allowed to adhere overnight. The following day, the medium was replaced with fresh medium containing 133 ng/ml of ^{125}I-labeled rat tail collagen I, and the cells were incubated for 5 h. Cells were washed three times in ice-cold PBS, trypsinized briefly, transferred to an Eppendorf tube, and centrifuged for 2 min at 200 *g*. Cells were then resuspended in DMEM with 10% FCS, reseeded in 6-well plates, and allowed to adhere for 0, 4, or 16 h. After this incubation, the culture supernatant was collected, and the cells were washed twice in PBS, briefly trypsinized, centrifuged at 200 *g* for 2 min, and resuspended in 1 ml of medium to neutralize the remaining trypsin. Cells were then centrifuged at 1,000 *g* for 1 min and lysed in lysis buffer (1% Triton X-100, 10 mM Tris, and 140 mM NaCl, pH 7.4). Subsequently, fresh medium was added to a total volume of 1 ml. Total protein content in either culture supernatant or lysates was precipitated by the addition of 90 µl of ice-cold 100% (wt/vol) TCA per milliliter and incubating the samples on ice for 10 min. Precipitated protein was separated from nonprecipitated material by centrifugation for 5 min at 12,000 *g*, and the amount of radioactivity in the fraction of precipitated protein (including intact nondegraded collagen) and nonprecipitated material (including degraded collagen) was determined using a γ counter.

Online supplemental material

Video 1 shows a reconstituted field of collagen formed in vivo. Table S1 shows the primers used for real-time PCR. Online supplemental material is available at http://www.jcb.org/cgi/content/full/jcb.201301081/DC1. Additional data are available in the JCB DataViewer at http://dx.doi.org/10.1083/jcb.201301081.dv.

We thank Drs. Silvio Gutkind and Mary Jo Danton for critically reviewing this manuscript.

Supported by the National Institute of Dental and Craniofacial Research Intramural Research Program (T.H. Bugge), the Lundbeck Foundation (D.H. Madsen), The Danish Cancer Society, the Danish Cancer Research Foundation, the Lundbeck Foundation, the Novo Nordisk Foundation, the Danish National Research Foundation (Danish-Chinese Center for Proteases and Cancer), the Grosserer Alfred Nielsen og Hustrus Foundation (L.H. Engelholm and

N. Behrendt), by a personal grant from Copenhagen University Hospital (H. J. Jürgensen), grants 5 R01 GM041804 and 2 P42 ES010337 (D.A. Brenner), and German Research Foundation (Deutsche Forschungsgemeinschaft) grant SFB645-C1 (S. Burgdorf).

Submitted: 21 January 2013
Accepted: 31 July 2013

References

Aimes, R.T., and J.P. Quigley. 1995. Matrix metalloproteinase-2 is an interstitial collagenase. Inhibitor-free enzyme catalyzes the cleavage of collagen fibrils and soluble native type I collagen generating the specific 3/4- and 1/4-length fragments. *J. Biol. Chem.* 270:5872–5876. http://dx.doi.org/10.1074/jbc.270.11.5872

Almholt, K., A. Juncker-Jensen, O.D. Laerum, K. Danø, M. Johnsen, L.R. Lund, and J. Rømer. 2008. Metastasis is strongly reduced by the matrix metalloproteinase inhibitor Galardin in the MMTV-PymT transgenic breast cancer model. *Mol. Cancer Ther.* 7:2758–2767. http://dx.doi.org/10.1158/1535-7163.MCT-08-0251

Arnold, L., A. Henry, F. Poron, Y. Baba-Amer, N. van Rooijen, A. Plonquet, R.K. Gherardi, and B. Chazaud. 2007. Inflammatory monocytes recruited after skeletal muscle injury switch into antiinflammatory macrophages to support myogenesis. *J. Exp. Med.* 204:1057–1069. http://dx.doi.org/10.1084/jem.20070075

Arora, P.D., M.F. Manolson, G.P. Downey, J. Sodek, and C.A. McCulloch. 2000. A novel model system for characterization of phagosomal maturation, acidification, and intracellular collagen degradation in fibroblasts. *J. Biol. Chem.* 275:35432–35441. http://dx.doi.org/10.1074/jbc.M003221200

Atabai, K., S. Jame, N. Azhar, A. Kuo, M. Lam, W. McKleroy, G. Dehart, S. Rahman, D.D. Xia, A.C. Melton, et al. 2009. Mfge8 diminishes the severity of tissue fibrosis in mice by binding and targeting collagen for uptake by macrophages. *J. Clin. Invest.* 119:3713–3722. http://dx.doi.org/10.1172/JCI40053

Beertsen, W., and V. Everts. 1977. The site of remodeling of collagen in the periodontal ligament of the mouse incisor. *Anat. Rec.* 189:479–497. http://dx.doi.org/10.1002/ar.1091890308

Berg, R.A., M.L. Schwartz, and R.G. Crystal. 1980. Regulation of the production of secretory proteins: intracellular degradation of newly synthesized "defective" collagen. *Proc. Natl. Acad. Sci. USA*. 77:4746–4750. http://dx.doi.org/10.1073/pnas.77.8.4746

Bienkowski, R.S., B.J. Baum, and R.G. Crystal. 1978. Fibroblasts degrade newly synthesised collagen within the cell before secretion. *Nature*. 276:413–416. http://dx.doi.org/10.1038/276413a0

Birkedal-Hansen, H., S. Yamada, J. Windsor, A.H. Poulsen, G. Lyons, W. Stetler-Stevenson, and B. Birkedal-Hansen. 2003. Matrix metalloproteinases. *Curr. Protoc. Cell Biol.* 10:10.8.1–10.8.23. http://dx.doi.org/10.1002/0471143030.cb1008s17

Bugge, T.H., and N. Behrendt. 2011. Cooperation between proteolysis and endocytosis in collagen turnover. *In* Extracellular Matrix Degradation. Vol. 2. W.C. Parks and R.P. Mecham, editors. Springer, Heidelberg, Germany. 53–74.

Bundesmann, M.M., T.E. Wagner, Y.H. Chow, W.A. Altemeier, T. Steinbach, and L.M. Schnapp. 2012. Role of urokinase plasminogen activator receptor-associated protein in mouse lung. *Am. J. Respir. Cell Mol. Biol.* 46:233–239. http://dx.doi.org/10.1165/rcmb.2010-0485OC

Cullen, J.C. 1972. Intracellular collagen in experimental arthritis in rats. *J. Bone Joint Surg. Br.* 54:351–359.

Curino, A.C., L.H. Engelholm, S.S. Yamada, K. Holmbeck, L.R. Lund, A.A. Molinolo, N. Behrendt, B.S. Nielsen, and T.H. Bugge. 2005. Intracellular collagen degradation mediated by uPARAP/Endo180 is a major pathway of extracellular matrix turnover during malignancy. *J. Cell Biol.* 169:977–985. http://dx.doi.org/10.1083/jcb.200411153

East, L., A. McCarthy, D. Wienke, J. Sturge, A. Ashworth, and C.M. Isacke. 2003. A targeted deletion in the endocytic receptor gene Endo180 results in a defect in collagen uptake. *EMBO Rep.* 4:710–716. http://dx.doi.org/10.1038/sj.embor.embor882

Engelholm, L.H., K. List, S. Netzel-Arnett, E. Cukierman, D.J. Mitola, H. Aaronson, L. Kjøller, J.K. Larsen, K.M. Yamada, D.K. Strickland, et al. 2003. uPARAP/Endo180 is essential for cellular uptake of collagen and promotes fibroblast collagen adhesion. *J. Cell Biol.* 160:1009–1015. http://dx.doi.org/10.1083/jcb.200211091

Everts, V., E. van der Zee, L. Creemers, and W. Beertsen. 1996. Phagocytosis and intracellular digestion of collagen, its role in turnover and remodelling. *Histochem. J.* 28:229–245. http://dx.doi.org/10.1007/BF02409011

Ezekowitz, R.A., D.J. Williams, H. Koziel, M.Y. Armstrong, A. Warner, F.F. Richards, and R.M. Rose. 1991. Uptake of *Pneumocystis carinii* mediated by the macrophage mannose receptor. *Nature*. 351:155–158. http://dx.doi.org/10.1038/351155a0

Fasquelle, C., A. Sartelet, W. Li, M. Dive, N. Tamma, C. Michaux, T. Druet, I.J. Huijbers, C.M. Isacke, W. Coppieters, et al. 2009. Balancing selection of a frame-shift mutation in the MRC2 gene accounts for the outbreak of the Crooked Tail Syndrome in Belgian Blue Cattle. *PLoS Genet.* 5:e1000666. http://dx.doi.org/10.1371/journal.pgen.1000666

Fässler, R., and M. Meyer. 1995. Consequences of lack of beta 1 integrin gene expression in mice. *Genes Dev.* 9:1896–1908. http://dx.doi.org/10.1101/gad.9.15.1896

Grobelny, D., L. Poncz, and R.E. Galardy. 1992. Inhibition of human skin fibroblast collagenase, thermolysin, and *Pseudomonas aeruginosa* elastase by peptide hydroxamic acids. *Biochemistry*. 31:7152–7154. http://dx.doi.org/10.1021/bi00146a017

Harris, E.D., Jr., A.M. Glauert, and A.H. Murley. 1977. Intracellular collagen fibers at the pannus-cartilage junction in rheumatoid arthritis. *Arthritis Rheum.* 20:657–665. http://dx.doi.org/10.1002/art.1780200204

Hotary, K., X.Y. Li, E. Allen, S.L. Stevens, and S.J. Weiss. 2006. A cancer cell metalloprotease triad regulates the basement membrane transmigration program. *Genes Dev.* 20:2673–2686. http://dx.doi.org/10.1101/gad.1451806

Joyce, J.A., and J.W. Pollard. 2009. Microenvironmental regulation of metastasis. *Nat. Rev. Cancer*. 9:239–252. http://dx.doi.org/10.1038/nrc2618

Jung, S., J. Aliberti, P. Graemmel, M.J. Sunshine, G.W. Kreutzberg, A. Sher, and D.R. Littman. 2000. Analysis of fractalkine receptor CX(3)CR1 function by targeted deletion and green fluorescent protein reporter gene insertion. *Mol. Cell. Biol.* 20:4106–4114. http://dx.doi.org/10.1128/MCB.20.11.4106-4114.2000

Jürgensen, H.J., D.H. Madsen, S. Ingvarsen, M.C. Melander, H. Gårdsvoll, L. Patthy, L.H. Engelholm, and N. Behrendt. 2011. A novel functional role of collagen glycosylation: interaction with the endocytic collagen receptor uparap/ENDO180. *J. Biol. Chem.* 286:32736–32748. http://dx.doi.org/10.1074/jbc.M111.266692

Jurukova, Z., and C. Milenkov. 1981. Involvement of smooth muscle cells in collagen degradation in the postpartum uterus. *Virchows Arch. B Cell Pathol. Incl. Mol. Pathol.* 37:237–244. http://dx.doi.org/10.1007/BF02892572

Kessenbrock, K., V. Plaks, and Z. Werb. 2010. Matrix metalloproteinases: regulators of the tumor microenvironment. *Cell*. 141:52–67. http://dx.doi.org/10.1016/j.cell.2010.03.015

Kjøller, L., L.H. Engelholm, M. Høyer-Hansen, K. Danø, T.H. Bugge, and N. Behrendt. 2004. uPARAP/endo180 directs lysosomal delivery and degradation of collagen IV. *Exp. Cell Res.* 293:106–116. http://dx.doi.org/10.1016/j.yexcr.2003.10.008

Krane, S.M., and M. Inada. 2008. Matrix metalloproteinases and bone. *Bone*. 43:7–18. http://dx.doi.org/10.1016/j.bone.2008.03.020

Krempen, K., D. Grotkopp, K. Hall, A. Bache, A. Gillan, R.A. Rippe, D.A. Brenner, and M. Breindl. 1999. Far upstream regulatory elements enhance position-independent and uterus-specific expression of the murine alpha1(I) collagen promoter in transgenic mice. *Gene Expr.* 8:151–163.

Lauer-Fields, J.L., D. Juska, and G.B. Fields. 2002. Matrix metalloproteinases and collagen catabolism. *Biopolymers*. 66:19–32. http://dx.doi.org/10.1002/bip.10201

Lecaille, F., D. Brömme, and G. Lalmanach. 2008. Biochemical properties and regulation of cathepsin K activity. *Biochimie*. 90:208–226. http://dx.doi.org/10.1016/j.biochi.2007.08.011

Lee, H., C.M. Overall, C.A. McCulloch, and J. Sodek. 2006. A critical role for membrane-type 1 matrix metalloproteinase in collagen phagocytosis. *Mol. Biol. Cell.* 17:4812–4826. http://dx.doi.org/10.1091/mbc.E06-06-0486

Lee, S.J., S. Evers, D. Roeder, A.F. Parlow, J. Risteli, L. Risteli, Y.C. Lee, T. Feizi, H. Langen, and M.C. Nussenzweig. 2002. Mannose receptor-mediated regulation of serum glycoprotein homeostasis. *Science*. 295:1898–1901. http://dx.doi.org/10.1126/science.1069540

Liu, X., H. Wu, M. Byrne, J. Jeffrey, S. Krane, and R. Jaenisch. 1995. A targeted mutation at the known collagenase cleavage site in mouse type I collagen impairs tissue remodeling. *J. Cell Biol.* 130:227–237. http://dx.doi.org/10.1083/jcb.130.1.227

Liu, S., S. Netzel-Arnett, H. Birkedal-Hansen, and S.H. Leppla. 2000. Tumor cell-selective cytotoxicity of matrix metalloproteinase-activated anthrax toxin. *Cancer Res.* 60:6061–6067.

López-Guisa, J.M., X. Cai, S.J. Collins, I. Yamaguchi, D.M. Okamura, T.H. Bugge, C.M. Isacke, C.L. Emson, S.M. Turner, S.J. Shankland, and A.A. Eddy. 2012. Mannose receptor 2 attenuates renal fibrosis. *J. Am. Soc. Nephrol.* 23:236–251. http://dx.doi.org/10.1681/ASN.2011030310

Lucattelli, M., E. Cavarra, M.M. de Santi, T.D. Tetley, P.A. Martorana, and G. Lungarella. 2003. Collagen phagocytosis by lung alveolar macrophages

in animal models of emphysema. *Eur. Respir. J.* 22:728–734. http://dx.doi.org/10.1183/09031936.03.00047603

Madsen, D.H., L.H. Engelholm, S. Ingvarsen, T. Hillig, R.A. Wagenaar-Miller, L. Kjøller, H. Gårdsvoll, G. Høyer-Hansen, K. Holmbeck, T.H. Bugge, and N. Behrendt. 2007. Extracellular collagenases and the endocytic receptor, urokinase plasminogen activator receptor-associated protein/Endo180, cooperate in fibroblast-mediated collagen degradation. *J. Biol. Chem.* 282:27037–27045. http://dx.doi.org/10.1074/jbc.M701088200

Madsen, D.H., S. Ingvarsen, H.J. Jürgensen, M.C. Melander, L. Kjøller, A. Moyer, C. Honoré, C.A. Madsen, P. Garred, S. Burgdorf, et al. 2011. The non-phagocytic route of collagen uptake: a distinct degradation pathway. *J. Biol. Chem.* 286:26996–27010. http://dx.doi.org/10.1074/jbc.M110.208033

Madsen, D.H., H. Jurgensen, S. Ingvarsen, M.C. Melander, B. Vainer, K.L. Egerod, A. Hald, B. Rønnø, C.A. Madsen, T.H. Bugge, et al. 2012. Endocytic collagen degradation: A novel mechanism involved in the protection against liver fibrosis. *J. Pathol.* 227:94–105. http://dx.doi.org/10.1002/path.3981

Malovic, I., K.K. Sørensen, K.H. Elvevold, G.I. Nedredal, S. Paulsen, A.V. Erofeev, B.H. Smedsrød, and P.A. McCourt. 2007. The mannose receptor on murine liver sinusoidal endothelial cells is the main denatured collagen clearance receptor. *Hepatology*. 45:1454–1461. http://dx.doi.org/10.1002/hep.21639

Martinez-Pomares, L., D. Wienke, R. Stillion, E.J. McKenzie, J.N. Arnold, J. Harris, E. McGreal, R.B. Sim, C.M. Isacke, and S. Gordon. 2006. Carbohydrate-independent recognition of collagens by the macrophage mannose receptor. *Eur. J. Immunol.* 36:1074–1082. http://dx.doi.org/10.1002/eji.200535685

Masedunskas, A., and R. Weigert. 2008. Intravital two-photon microscopy for studying the uptake and trafficking of fluorescently conjugated molecules in live rodents. *Traffic*. 9:1801–1810. http://dx.doi.org/10.1111/j.1600-0854.2008.00798.x

Messaritou, G., L. East, C. Roghi, C.M. Isacke, and H. Yarwood. 2009. Membrane type-1 matrix metalloproteinase activity is regulated by the endocytic collagen receptor Endo180. *J. Cell Sci.* 122:4042–4048. http://dx.doi.org/10.1242/jcs.044305

Mosser, D.M., and J.P. Edwards. 2008. Exploring the full spectrum of macrophage activation. *Nat. Rev. Immunol.* 8:958–969. http://dx.doi.org/10.1038/nri2448

Neurath, M.F. 1993. Detection of Luse bodies, spiralled collagen, dysplastic collagen, and intracellular collagen in rheumatoid connective tissues: an electron microscopic study. *Ann. Rheum. Dis.* 52:278–284. http://dx.doi.org/10.1136/ard.52.4.278

Otter, M., J. Kuiper, R. Bos, D.C. Rijken, and T.J. van Berkel. 1992. Characterization of the interaction both in vitro and in vivo of tissue-type plasminogen activator (t-PA) with rat liver cells. Effects of monoclonal antibodies to t-PA. *Biochem. J.* 284:545–550.

Panchuk-Voloshina, N., R.P. Haugland, J. Bishop-Stewart, M.K. Bhalgat, P.J. Millard, F. Mao, W.Y. Leung, and R.P. Haugland. 1999. Alexa dyes, a series of new fluorescent dyes that yield exceptionally bright, photostable conjugates. *J. Histochem. Cytochem.* 47:1179–1188. http://dx.doi.org/10.1177/002215549904700910

Paveley, R.A., S.A. Aynsley, J.D. Turner, C.D. Bourke, S.J. Jenkins, P.C. Cook, L. Martinez-Pomares, and A.P. Mountford. 2011. The Mannose Receptor (CD206) is an important pattern recognition receptor (PRR) in the detection of the infective stage of the helminth *Schistosoma mansoni* and modulates IFNγ production. *Int. J. Parasitol.* 41:1335–1345. http://dx.doi.org/10.1016/j.ijpara.2011.08.005

Prigozy, T.I., P.A. Sieling, D. Clemens, P.L. Stewart, S.M. Behar, S.A. Porcelli, M.B. Brenner, R.L. Modlin, and M. Kronenberg. 1997. The mannose receptor delivers lipoglycan antigens to endosomes for presentation to T cells by CD1b molecules. *Immunity*. 6:187–197. http://dx.doi.org/10.1016/S1074-7613(00)80425-2

Rowe, R.G., and S.J. Weiss. 2009. Navigating ECM barriers at the invasive front: the cancer cell-stroma interface. *Annu. Rev. Cell Dev. Biol.* 25:567–595. http://dx.doi.org/10.1146/annurev.cellbio.24.110707.175315

Royer, P.J., M. Emara, C. Yang, A. Al-Ghouleh, P. Tighe, N. Jones, H.F. Sewell, F. Shakib, L. Martinez-Pomares, and A.M. Ghaemmaghami. 2010. The mannose receptor mediates the uptake of diverse native allergens by dendritic cells and determines allergen-induced T cell polarization through modulation of IDO activity. *J. Immunol.* 185:1522–1531. http://dx.doi.org/10.4049/jimmunol.1000774

Ryvnyak, V.V., and O.F. Dulgieru. 2003. Elastase involvement in extracellular and intracellular collagen degradation during postpartum involution of the uterus. *Bull. Exp. Biol. Med.* 136:206–208. http://dx.doi.org/10.1023/A:1026395613444

Sandoval, R.M., M.D. Kennedy, P.S. Low, and B.A. Molitoris. 2004. Uptake and trafficking of fluorescent conjugates of folic acid in intact kidney determined using intravital two-photon microscopy. *Am. J. Physiol. Cell Physiol.* 287:C517–C526. http://dx.doi.org/10.1152/ajpcell.00006.2004

Schnack Nielsen, B., F. Rank, L.H. Engelholm, A. Holm, K. Danø, and N. Behrendt. 2002. Urokinase receptor-associated protein (uPARAP) is expressed in connection with malignant as well as benign lesions of the human breast and occurs in specific populations of stromal cells. *Int. J. Cancer*. 98:656–664. http://dx.doi.org/10.1002/ijc.10227

Segal, G., W. Lee, P.D. Arora, M. McKee, G. Downey, and C.A. McCulloch. 2001. Involvement of actin filaments and integrins in the binding step in collagen phagocytosis by human fibroblasts. *J. Cell Sci.* 114:119–129.

Segovia-Silvestre, T., A.V. Neutzsky-Wulff, M.G. Sorensen, C. Christiansen, J. Bollerslev, M.A. Karsdal, and K. Henriksen. 2009. Advances in osteoclast biology resulting from the study of osteopetrotic mutations. *Hum. Genet.* 124:561–577. http://dx.doi.org/10.1007/s00439-008-0583-8

Sheikh, H., H. Yarwood, A. Ashworth, and C.M. Isacke. 2000. Endo180, an endocytic recycling glycoprotein related to the macrophage mannose receptor is expressed on fibroblasts, endothelial cells and macrophages and functions as a lectin receptor. *J. Cell Sci.* 113:1021–1032.

Sica, A., P. Larghi, A. Mancino, L. Rubino, C. Porta, M.G. Totaro, M. Rimoldi, S.K. Biswas, P. Allavena, and A. Mantovani. 2008. Macrophage polarization in tumour progression. *Semin. Cancer Biol.* 18:349–355. http://dx.doi.org/10.1016/j.semcancer.2008.03.004

Soames, J.V., and R.M. Davies. 1977. Intracellular collagen fibrils in early gingivitis in the beagle dog. *J. Periodontal Res.* 12:378–386. http://dx.doi.org/10.1111/j.1600-0765.1977.tb01528.x

Stephens, L.E., A.E. Sutherland, I.V. Klimanskaya, A. Andrieux, J. Meneses, R.A. Pedersen, and C.H. Damsky. 1995. Deletion of beta 1 integrins in mice results in inner cell mass failure and peri-implantation lethality. *Genes Dev.* 9:1883–1895. http://dx.doi.org/10.1101/gad.9.15.1883

Sulek, J., R.A. Wagenaar-Miller, J. Shireman, A. Molinolo, D.H. Madsen, L.H. Engelholm, N. Behrendt, and T.H. Bugge. 2007. Increased expression of the collagen internalization receptor uPARAP/Endo180 in the stroma of head and neck cancer. *J. Histochem. Cytochem.* 55:347–353. http://dx.doi.org/10.1369/jhc.6A7133.2006

Tan, M.C., A.M. Mommaas, J.W. Drijfhout, R. Jordens, J.J. Onderwater, D. Verwoerd, A.A. Mulder, A.N. van der Heiden, T.H. Ottenhoff, M. Cella, et al. 1997. Mannose receptor mediated uptake of antigens strongly enhances HLA-class II restricted antigen presentation by cultured dendritic cells. *Adv. Exp. Med. Biol.* 417:171–174. http://dx.doi.org/10.1007/978-1-4757-9966-8_28

Wagenaar-Miller, R.A., L.H. Engelholm, J. Gavard, S.S. Yamada, J.S. Gutkind, N. Behrendt, T.H. Bugge, and K. Holmbeck. 2007. Complementary roles of intracellular and pericellular collagen degradation pathways in vivo. *Mol. Cell. Biol.* 27:6309–6322. http://dx.doi.org/10.1128/MCB.00291-07

Wang, H.W., and J.A. Joyce. 2010. Alternative activation of tumor-associated macrophages by IL-4: priming for protumoral functions. *Cell Cycle*. 9:4824–4835. http://dx.doi.org/10.4161/cc.9.24.14322

Wienke, D., J.R. MacFadyen, and C.M. Isacke. 2003. Identification and characterization of the endocytic transmembrane glycoprotein Endo180 as a novel collagen receptor. *Mol. Biol. Cell*. 14:3592–3604. http://dx.doi.org/10.1091/mbc.E02-12-0814

Wienke, D., G.C. Davies, D.A. Johnson, J. Sturge, M.B. Lambros, K. Savage, S.E. Elsheikh, A.R. Green, I.O. Ellis, D. Robertson, et al. 2007. The collagen receptor Endo180 (CD280) Is expressed on basal-like breast tumor cells and promotes tumor growth in vivo. *Cancer Res.* 67:10230–10240. http://dx.doi.org/10.1158/0008-5472.CAN-06-3496